QCD chiral transition, $U(1)_A$ symmetry and the dirac spectrum using domain wall fermions

Michael I. Buchoff,[1,2] Michael Cheng,[3] Norman H. Christ,[4] H.-T. Ding,[4,5] Chulwoo Jung,[5] F. Karsch,[5,6] Zhongjie Lin,[4] R. D. Mawhinney,[4] Swagato Mukherjee,[5] P. Petreczky,[5] Dwight Renfrew,[4] Chris Schroeder,[1] P. M. Vranas,[1] Hantao Yin[4]

(LLNL/RBC Collaboration)

[1]*Physics Division, Lawrence Livermore National Laboratory, Livermore, California 94550, USA*
[2]*Institute for Nuclear Theory, Box 351550, Seattle, Washington 98195-1550, USA*
[3]*Center for Computational Science, Boston University, Boston, Massachusetts 02215, USA*
[4]*Physics Department, Columbia University, New York, New York 10027, USA*
[5]*Physics Department, Brookhaven National Laboratory, Upton, New York 11973, USA*
[6]*Fakultät für Physik, Universität Bielefeld, D-33615 Bielefeld, Germany*

We report on a study of the finite-temperature QCD transition region for temperatures between 139 and 196 MeV, with a pion mass of 200 MeV and two space-time volumes: $24^3 \times 8$ and $32^3 \times 8$, where the larger volume varies in linear size between 5.6 fm (at $T = 139$ MeV) and 4.0 fm (at $T = 195$ MeV). These results are compared with the results of an earlier calculation using the same action and quark masses but a smaller, $16^3 \times 8$ volume. The chiral domain wall fermion formulation with a combined Iwasaki and dislocation suppressing determinant ratio gauge action are used. This lattice action accurately reproduces the $SU(2)_L \times SU(2)_R$ and $U(1)_A$ symmetries of the continuum. Results are reported for the chiral condensates, connected and disconnected susceptibilities and the Dirac eigenvalue spectrum. We find a pseudocritical temperature, T_c, of approximately 165 MeV consistent with previous results and strong finite-volume dependence below T_c. Clear evidence is seen for $U(1)_A$ symmetry breaking above T_c which is quantitatively explained by the measured density of near-zero modes in accordance with the dilute instanton gas approximation.

I. INTRODUCTION

The QCD phase transition, separating the low-temperature phase in which the (approximate) $SU(2)_L \times SU(2)_R$ symmetry of QCD with two light flavors is broken by the vacuum and the high-temperature phase in which this symmetry is restored, has been the subject of active experimental and theoretical study for more than 30 years. The present expectation is that this is a second-order transition belonging to the $O(4)$ universality class when the up and down quark masses are zero [1] and a possibly rapid cross over for nonzero, physical light-quark mass.

However, the order of the transition may depend on the degree to which the anomalous $U(1)_A$ symmetry is realized in QCD. As pointed out in Ref. [1], if the $U(1)_A$ breaking is significant near the phase transition, then the resulting four massless degrees of freedom ($\vec{\pi}$ and σ) can support $O(4)$ critical behavior at T_c, the location of the phase transition. However, if anomalous breaking of the $U(1)_A$ is small so there are eight light degrees of freedom at T_c ($\vec{\pi}, \sigma, \vec{\delta}$ and η) then the chiral transition is expected to be first order, although a second-order phase transition may still be permitted with a different $SU(2)_L \times SU(2)_R/U(2)_V$ universality class as suggested in Refs. [2,3]. Thus, a thorough

study of the behavior of the anomalous $U(1)_A$ symmetry has essential consequences on the nature of the chiral phase transition. (For a recent investigation of this question using an effective Lagrangian approach see Ref. [4].)

In this paper we study the temperature region 139 MeV $\leq T \leq$ 195 MeV using chiral, domain wall fermions (DWF) with a lattice volume having a fixed time extent of 8 in lattice units and a spatial volume of either 24^3 or 32^3. The temperature is varied by varying the inverse gauge coupling β between 1.633 and 1.829 using the Iwasaki gauge action combined with a dislocation suppressing determinant ratio (DSDR) [5–8] to reduce the effects of residual chiral symmetry breaking at these relatively strong couplings. The light-quark mass is chosen so that the pion mass is held fixed at a heavier-than-physical 200 MeV value while the strange quark mass is set to its physical value. This calculation extends previous work [9] that used the same action and studied the same quark masses and temperatures but used a smaller $16^3 \times 8$ volume.

While the QCD phase transition has been extensively studied using the staggered formulation of lattice fermions, calculations employing chiral fermions are more difficult and less frequent [9–13]. However, in contrast to the

staggered formulation in which finite lattice spacing effects explicitly break the anomalous $U(1)_A$ symmetry and all but one of the six $SU(2)_L \times SU(2)_R$ symmetry directions, the DWF formulation accurately reproduces these symmetries. At low temperatures one finds three degenerate light pions and the $U(1)_A$ current obeys an anomalous conservation law identical to that in the continuum up to small, controlled residual chiral symmetry breaking effects.

We will now briefly summarize our results. The disconnected chiral susceptibility χ_{disc} shows a dramatic peak as the temperature increases through the critical region. This is the quantity of choice for locating the pseudocritical temperature and showed a quite broad peak when studied earlier on the $16^3 \times 8$ volume. The 24^3 and 32^3 results presented here show a significant volume dependence with the large shoulder just below T_c decreasing by between 30% and 50% as the volume is increased and the peak itself moving to higher temperature and decreasing in height by approximately 15%. The 24^3 and 32^3 volumes give similar results. This behavior is predicted by finite size scaling in $O(4)$ models in the presence of an external symmetry breaking field [14] and could be anticipated from the first comparison made with QCD data [15] and the recent work of Braun *et al.* [16].

We investigate $U(1)_A$ symmetry breaking above T_c by examining the two $U(1)_A$ symmetry breaking differences $\chi_\pi - \chi_\delta$ and $\chi_\sigma - \chi_\eta$. These vanish if $U(1)_A$ symmetry is realized and are clearly nonzero at $T = 177$ MeV, although they decrease quickly as T is increased above this value. These two quantities are related by $SU(2)_L \times SU(2)_R$ symmetry and are equal within errors for $T \geq 177$ MeV. We conclude that for temperatures at which $SU(2)_L \times SU(2)_R$ symmetry has been restored, $U(1)_A$ symmetry breaking is still present.

The Dirac eigenvalue spectra per unit space-time volume seen on the $16^3 \times 8$ and $32^3 \times 8$ volumes are very similar. However, the larger volume results are more accurate in the region of small eigenvalues. We find that appropriately convergent combinations of spectral integrals agree well with the observed Green's functions to which they are related in continuum field theory. Of particular importance is the agreement between a spectral integral and $\chi_\pi - \chi_\delta$. For $T = 177$ MeV we find a small cluster of near-zero Dirac eigenvalues, such as are expected from the dilute instanton gas approximation (DIGA) [17,18] and it is these eigenvalues which, when included in the spectral formula, reproduce the measured result for $\chi_\pi - \chi_\delta$. This relation continues to hold, although within larger errors, at $T = 186$ and 195 MeV. The number of these near-zero modes is found to be proportional to the volume and their chiralities show a mixture of positive and negative values per configuration, as is expected in the DIGA. We conclude that $U(1)_A$ symmetry is broken in the region immediately above T_c and this breaking is explained by the DIGA. No additional mechanism is necessary.

In addition to these physics results, we also present two technical improvements to the study of finite-temperature phenomena using DWF. The first is an improved observable representing the chiral condensate, $\langle \bar{\psi}_l \psi_l \rangle$. This new quantity, the difference of light and strange quark chiral susceptibilities, is equivalent in the continuum to the usual difference of light and strange quark condensates but does not contain the residual chiral symmetry breaking ambiguities present in the usual DWF evaluation of such a difference. The second development is the recognition that the quantities usually computed when evaluating susceptibilities and computing residual DWF chiral symmetry breaking, and hence fundamental to this and earlier calculations, are related by an exact DWF Ward identity and the demonstration that this relation is satisfied.

This paper is organized as follows. Section II briefly describes the lattice formulation used, ensembles generated and the input parameters chosen. In Sec. III, we introduce a variety of observables that are associated with the $SU(2)_L \times SU(2)_R$ and $U(1)_A$ symmetries and review their properties and the symmetry relations that connect them. We present and discuss the results for these observables over our 139–195 MeV temperature range. Section IV gives results for the low-lying eigenvalue spectrum of the Dirac operator and examines the relations between this spectrum and various measures of the chiral condensate and $\chi_\pi - \chi_\delta$. Finally in Sec. V, we summarize our results and compare with earlier work.

II. ENSEMBLE DETAILS

In this calculation we extend the $16^3 \times 8$ results reported in Ref. [9] to larger $24^3 \times 8$ and $32^3 \times 8$ volumes, keeping all other parameters fixed. We therefore adopt the same Iwasaki gauge action augmented with the DSDR [6–8] and the DWF action with $2 + 1$ flavors. With this choice of action, we are able to simulate a relatively light pion mass and to accurately respect the important continuum chiral and $U(1)_A$ symmetries.

Table I lists the basic parameters for these three sets of ensembles. The first two sets of ensembles are new and reported here for the first time, with space-time volumes of $32^3 \times 8$ and $24^3 \times 8$ respectively. The third set of ensembles, with lattice volume $16^3 \times 8$, was studied extensively in Ref. [9] and is listed here [with improved statistics at $T = 195$ MeV (run #21)] for comparison and later reference.

The input light-quark masses are adjusted so that all the ensembles lie on a line of constant physics with $m_\pi \approx 200$ MeV and the ratio $\tilde{m}_l / \tilde{m}_s = 0.088$ is fixed to ensure a kaon with physical mass. Here and later in the text, a tilde indicates the total bare quark mass, given by the sum of the input and the residual quark masses $\tilde{m} = m_{\text{input}} + m_{\text{res}}$, where the residual mass, m_{res} is the small additive shift to the input quark mass that results from the residual chiral symmetry breaking with DWF with a finite extent L_s in the

TABLE I. Summary of input parameters (β, N_σ, N_τ, L_s, m_l and m_s) and the measured result for $m_{\rm res}$ for each ensembles. Each is assigned a label in the first column for later reference. The final $N_{\rm traj}^{\rm equil}$ column lists the number of equilibrated trajectories that remain after the imposition of the thermalization and decorrelation cuts described in the text.

#	T (MeV)	β	N_σ	N_τ	L_s	m_l	m_s	$m_{\rm res}$	m_π (MeV)	$N_{\rm traj}^{\rm equil}$
1	139(6)	1.633	32	8	48	−0.00136	0.0519	0.00657(2)	205(8)	2700
2	149(5)	1.671	32	8	32	−0.00189	0.0464	0.00653(2)	201(5)	2700
3	159(4)	1.707	32	8	32	0.000551	0.0449	0.00366(2)	200(3)	2643
4	164(4)	1.725	32	8	32	0.00138	0.0436	0.00277(1)	202(3)	2700
5	168(4)	1.740	32	8	32	0.00175	0.0427	0.00220(2)	200(2)	2708
6	177(4)	1.771	32	8	32	0.00232	0.0403	0.00135(1)	198(2)	2700
7	186(5)	1.801	32	8	32	0.00258	0.0379	0.00083(2)	197(3)	2729
8	195(6)	1.829	32	8	32	0.00265	0.0357	0.00049(1)	195(4)	3112
9	149(5)	1.671	24	8	32	−0.00189	0.0464	0.00659(6)	202(5)	4721
10	159(4)	1.707	24	8	32	0.000551	0.0449	0.00370(4)	200(3)	2265
11	168(4)	1.740	24	8	32	0.00175	0.0427	0.00216(3)	199(2)	2423
12	177(4)	1.771	24	8	32	0.00232	0.0403	0.00129(3)	197(2)	2892
13	186(5)	1.801	24	8	32	0.00258	0.0379	0.00084(3)	197(3)	3142
14	139(6)	1.633	16	8	48	−0.00136	0.0519	0.00588(39)	191(7)	2696
15	149(5)	1.671	16	8	32	−0.00189	0.0464	0.00643(9)	199(5)	5700
16	149(5)	1.671	16	8	48	0.00173	0.0500	0.00295(3)	202(5)	6700
17	159(4)	1.707	16	8	32	0.000551	0.0449	0.00377(11)	202(3)	3359
18	168(4)	1.740	16	8	32	0.00175	0.0427	0.00209(9)	197(2)	3043
19	177(4)	1.771	16	8	32	0.00232	0.0403	0.00132(6)	198(2)	3240
20	186(5)	1.801	16	8	32	0.00258	0.0379	0.00076(3)	195(3)	4415
21	195(6)	1.829	16	8	32	0.00265	0.0357	0.00047(1)	194(4)	8830

fifth dimension. A detailed description of the determination of the line of constant physics can be found in Ref. [9]. Here we recalculate the pion masses at each temperature from updated values of the residual mass computed on the $32^3 \times 8$ and $24^3 \times 8$ ensembles. As can be seen in column nine of Table I, in all but one case these new values for m_π lie within 3% of the target value of 200 MeV. Determined as it is here from the sum of input and residual light-quark masses and the assumed linearity of m_π^2 on this sum, the pion mass should be independent of the volume and the difference of the calculated pion masses between different volumes can be regarded as a measure of systematic errors.

Because of the rapidly increasing residual mass with decreasing temperature, for the two lowest temperature ensembles ($T = 139$ and 149 MeV), we use a negative input quark mass. While much larger negative input quark masses are standard for Wilson fermion calculations, the use of negative $m_{\rm input}$ is uncommon in a DWF calculation and, as in the Wilson case, could potentially jeopardize the stability of the evolution because of a singularity in the Dirac operator. Fortunately, we observed no such "exceptional configurations" in any of our evolutions. This use of a negative input quark mass was tested in a study reported in Ref. [9] where two streams at $T = 149$ MeV with a $16^3 \times 8$ volume were generated: one with $L_s = 32$ and a negative input quark mass (run #15 in Table I) and a second with $L_s = 48$ and a positive input quark mass (run #16 in Table I), adjusted to give the same value of $\tilde{m}_l$. Both ensembles gave consistent results for all the quantities we computed, providing strong support that

our interpretation of $\tilde{m}_l$ and choice of negative input quark mass is solid and correct.

The number of effective trajectories for each ensemble that are used in the measurement reported later is also in the rightmost column of Table I. For ensembles with volume $16^3 \times 8$ and $32^3 \times 8$, we discard the first 300 trajectories to account for thermalization. However, because we changed the evolution algorithm during the early stages of the generation of the $24^3 \times 8$ ensembles, a larger number of initial trajectories were discarded for those. For each ensemble a trajectory has a length of one molecular dynamics time unit.

In order to increase the statistics, we have evolved multiple streams for ensembles run #9 and run #10. Ensemble run #9 is composed of 8 streams, two of which began from an ordered start, another two from a disordered start and the remaining four were split from the previous four streams after thermalization. Ensemble run #10 is composed of two streams, one beginning from an ordered and the other from a disordered configuration. The multiple streams in each ensemble are pooled together after removing an initial 300 trajectories from each stream which began with an ordered or disordered start. For streams that were split from a previously thermalized stream, the first 100 trajectories of that new stream are discarded to insure that the new stream is not correlated with its parent.

We do not adopt a single set of units in this paper. When dimensionful quantities are given in physical units, such as MeV, the unit used will be specified. However, when expressed in lattice units, often no explicit unit will be written. Occasionally, for clarity or emphasis, explicit powers of the lattice spacing will be shown, with the

power given by the length dimension of the quantity being described.

III. CHIRAL OBSERVABLES

In this section we will discuss Green's functions constructed from the eight scalar and pseudoscalar operators: $\bar{\psi}_l\psi_l$, $\bar{\psi}_l\tau^i\psi_l$, $\bar{\psi}_l\gamma^5\psi_l$, $\bar{\psi}_l\tau^i\gamma^5\psi_l$. Here ψ_l is a doublet of up and down quark fields and $\{\tau_i\}_{1\leq i\leq 3}$ the usual Pauli matrices. These operators are related by the $SU(2)_L \times SU(2)_R$ chiral symmetry of QCD and the anomalously broken $U(1)_A$ symmetry. In Sec. III A we review the relations among these eight operators and their Green's functions implied by the $SU(2)_L \times SU(2)_R$ and $U(1)_A$ symmetries, paying particular attention to the degree to which these relations should hold at finite lattice spacing for the DWF formulation.

In Sec. III B we present our numerical results, focusing on those relations implied by $SU(2) \times SU(2)$ chiral symmetry and examining their dependence on temperature. In the final subsection, Sec. III C, we examine the relations implied by $U(1)_A$ symmetry, including evidence for nonzero anomalous, $U(1)_A$ symmetry breaking above the pseudocritical temperature T_c, a nonvanishing asymmetry which disappears rapidly as the temperature increases above T_c.

A. Preliminaries

In this section, we present a brief review of a variety of chiral observables and the relations among them implied by the $SU(2)_L \times SU(2)_R$ and $U(1)_A$ symmetries. A more detailed description can be found in Ref. [9].

The standard order parameter for the chiral phase transition is the single-flavor, light-quark chiral condensate,

$$\Sigma_l \equiv -\frac{1}{2}\langle\bar{\psi}_l\psi_l\rangle \tag{1}$$

$$= \frac{1}{2}\frac{T}{V}\frac{\partial \ln Z}{\partial m_l} \tag{2}$$

$$= \frac{1}{N_\sigma^3 N_\tau}\langle\mathrm{Tr}M_l^{-1}\rangle, \tag{3}$$

where M_l is the single-flavor, light-quark Dirac matrix and the brackets $\langle\ldots\rangle$ in the bottom equation indicate an average over gauge fields. However, this quantity contains an ultraviolet divergent contribution that is proportional to m_q/a^2 for the case of a lattice regularization. In order to remove this ultraviolet divergence, it is standard to introduce a subtracted chiral condensate constructed from a weighted difference between the chiral condensates of the light and strange quarks [19]:

$$\Delta_{l,s} = \Sigma_l - \frac{\tilde{m}_l}{\tilde{m}_s}\Sigma_s. \tag{4}$$

Here Σ_s is defined using the strange quark Dirac matrix in a manner analogous to Eq. (3). For domain wall fermions there is a further difficulty associated with the short distance contributions to Σ_q and the subtracted quantity $\Delta_{l,s}$. For a finite fifth dimensional extent, $L_s < \infty$, the DWF chiral symmetry is only approximate and residual chirally symmetry breaking effects appear. The largest such effect is a small additive shift in the quark mass: the residual mass m_{res} mentioned above. Similar residual chiral breaking will appear in Σ_q and will be of order m_{res}/a^2 if we express m_{res} in physical units. However, since the detailed mechanism which generates the residual mass is not directly related to that which introduces the additive constant into Σ_q, the subtraction coefficient α that would be needed to remove both the m_q/a^2 and the $O(m_{\mathrm{res}}/a^2)$ terms in $\Sigma_l - \alpha\Sigma_s$ is not known.

Thus, the subtracted quantity $\Delta_{l,s}$ defined in Eq. (4) will contain an unphysical, $O(m_{\mathrm{res}}/a^2)$ constant which will decrease the utility of $\Delta_{l,s}$ computed in a DWF simulation. In particular, we cannot compare $\Delta_{l,s}$ with the same difference of chiral condensates obtained from other lattice fermion formulations. While this added unphysical constant does not depend on temperature, it does depend strongly on the gauge coupling g so the usual procedure of varying the temperature by varying g at fixed N_τ will induce an apparent temperature dependence in this unphysical contribution to $\Delta_{l,s}$. However, the definition of $\Delta_{l,s}$ given in Eq. (4) (which differs from that used in the earlier paper [9]) does have a useful property. As is discussed in Sec. IV, this subtraction using for α the physical quark mass ratio, $\alpha = \tilde{m}_l/\tilde{m}_s$ will lead to a more convergent spectral expression for $\Delta_{l,s}$.

Results for the quantities Σ_l, Σ_s and $\Delta_{l,s}$ are given in Table III. For each configuration used in the calculation, the volume-averaged, chiral condensate is computed from the right-hand side of Eq. (3), using 10 Gaussian random volume sources to estimate the trace. In Sec. III we will use the Gell-Mann-Oakes-Renner (GMOR) relation to define an improved, subtracted chiral condensate $\tilde{\Delta}_{l,s}$, which contains a much smaller unknown correction and can be compared with the results from other formulations of lattice fermions.

The chiral condensate Σ_l and the various subtracted versions discussed above can be used to explore the vacuum breaking of $SU(2)_L \times SU(2)_R$ and $U(1)_A$ symmetry and their restoration (or partial restoration) as the temperature is increased. However, much more information can be obtained from the susceptibilities defined as integrated correlation functions of the eight local operators,

$$\sigma = \bar{\psi}_l\psi_l \tag{5}$$

$$\delta^i = \bar{\psi}_l\tau^i\psi_l \tag{6}$$

$$\eta = i\bar{\psi}_l\gamma^5\psi_l \tag{7}$$

$$\pi^i = i\bar{\psi}_l\tau^i\gamma^5\psi_l. \tag{8}$$

Such susceptibilities are both much more sensitive to the transition from the ordered to the disordered state and also allow independent measures of $SU(2)_L \times SU(2)_R$ and $U(1)_A$ symmetry breaking. The operator quadruplets (σ, π^i) and (η, δ^i) each transform as an irreducible four-dimensional representation of $SU(2)_L \times SU(2)_R$. The four pairs, (σ, η), $(\delta^i, \pi^i)_{1 \leq i \leq 3}$ each transform the simple, two-dimensional representation of $U(1)_A$. We then identify the four distinct susceptibilities which are allowed by isospin symmetry:

$$\chi_\sigma = \frac{1}{2}\int d^4x \langle \sigma(x)\sigma(0)\rangle \tag{9}$$

$$\chi_\delta = \frac{1}{2}\int d^4x \langle \delta^i(x)\delta^i(0)\rangle \tag{10}$$

$$\chi_\eta = \frac{1}{2}\int d^4x \langle \eta(x)\eta(0)\rangle \tag{11}$$

$$\chi_\pi = \frac{1}{2}\int d^4x \langle \pi^i(x)\pi^i(0)\rangle, \tag{12}$$

where the factor $1/2$ has been introduced so that these correspond to the single-flavor quantities that are typically computed using lattice methods and no sum over the repeated index i is intended. In light of the multiplet structure defined above, the following relations are implied by $SU(2)_L \times SU(2)_R$ and $U(1)_A$ symmetry:

$$\left.\begin{array}{rcl}\chi_\sigma &=& \chi_\pi \\ \chi_\eta &=& \chi_\delta\end{array}\right\} \quad SU(2)_L \times SU(2)_R, \tag{13}$$

$$\left.\begin{array}{rcl}\chi_\sigma &=& \chi_\eta \\ \chi_\pi &=& \chi_\delta\end{array}\right\} \quad U(1)_A. \tag{14}$$

These susceptibilities can be written in terms of the Dirac operator M_l. For the correlators of the operators π^i and δ^i, which introduce nonzero isospin, only connected combinations appear:

$$\chi_\pi = \frac{1}{N_\sigma^3 N_\tau}\mathrm{Tr}\langle\gamma^5 M_l^{-1}\gamma^5 M_l^{-1}\rangle \tag{15}$$

$$\chi_\delta = -\frac{1}{N_\sigma^3 N_\tau}\mathrm{Tr}\langle M_l^{-1}M_l^{-1}\rangle, \tag{16}$$

where the notation "Tr" indicates a trace over spinor and color indices as well as the space-time volume. The σ and η susceptibilities are a combination of the connected parts which appear in χ_δ and χ_π respectively and a disconnected part:

$$\chi_\sigma = \chi_\delta + 2\chi_{\mathrm{disc}} \tag{17}$$

$$\chi_\eta = \chi_\pi - 2\chi_{5,\mathrm{disc}}, \tag{18}$$

where the disconnected parts χ_{disc} and $\chi_{5,\mathrm{disc}}$ are given by

$$\chi_{\mathrm{disc}} = \frac{1}{N_\sigma^3 N_\tau}\{\langle(\mathrm{Tr}M_l^{-1})^2\rangle - (\langle\mathrm{Tr}M_l^{-1}\rangle)^2\} \tag{19}$$

$$\chi_{5,\mathrm{disc}} = \frac{1}{N_\sigma^3 N_\tau}\langle(\mathrm{Tr}M_l^{-1}\gamma^5)^2\rangle. \tag{20}$$

As is conventional, we have removed the truly disconnected piece $2N_s^3 N_\tau\Sigma_l^2$ from the expression for χ_σ given in Eq. (17). This extra term would appear if the right-hand side of the definition given by Eq. (9) were completely evaluated. The factor of 2 that appears in Eqs. (17) and (18) was mistakenly omitted from the published version of Ref. [9] and arises when these relations are written in terms of single-flavor quantities. The signs of χ_{disc} and $\chi_{5,\mathrm{disc}}$ have been chosen so that each is positive.

We can combine Eqs. (13), (17) and (18) to obtain relations between the $U(1)_A$ symmetry breaking difference $\chi_\pi - \chi_\delta$ and χ_{disc} and $\chi_{5,\mathrm{disc}}$ if $SU(2)_L \times SU(2)_R$ symmetry is assumed:

$$\chi_\pi - \chi_\delta = (\chi_\pi - \chi_\sigma) + (\chi_\sigma - \chi_\delta) \tag{21}$$

$$= 2\chi_{\mathrm{disc}} \tag{22}$$

$$= 2\chi_{5,\mathrm{disc}}, \tag{23}$$

where the second equation is true if the $SU(2)_L \times SU(2)_R$ relation $\chi_\pi = \chi_\sigma$ of Eq. (13) is valid while the third is obtained by a similar manipulation and the second $SU(2)_L \times SU(2)_R$ relation $\chi_\delta = \chi_\eta$.

The connected Green's functions can be computed from the lattice by integrating the two-point correlators from a point source over the whole volume. This method was used for the calculations on the $24^3 \times 8$ ensembles as well as our earlier study of the $16^3 \times 8$ ensembles in [9]. On the $32^3 \times 8$ ensembles and for the $16^3 \times 8$ results presented in this report, we achieved a reduced statistical error by using instead a random Z_2 wall source. The disconnected parts are calculated by averaging products of chiral condensates where the stochastic evaluation of the trace appearing in each factor is obtained from different stochastic sources.

The $SU(2)_L \times SU(2)_R$ relations given in Eq. (13) should be valid in the continuum for $T > T_c$ when $SU(2)_L \times SU(2)_R$ becomes an accurate symmetry. They should also be true when $T > T_c$ in a lattice formulation which preserves chiral symmetry. However, for our DWF formulation we should expect deviations arising from residual chiral symmetry breaking. For low-energy quantities,

$m_{\rm res}$ should provide a good measure of this residual chiral symmetry breaking, with effects that are well described as arising simply from the total bare quark mass $\tilde{m} = m_l + m_{\rm res}$.

However, the four susceptibilities being discussed are not simple long-distance quantities since the space-time integrals that appear in their definitions include points where the two local operators collide. In fact, the connected parts of the susceptibilities contain quadratic divergences while the disconnected parts diverge logarithmically. The presence of quadratic divergences in the connected susceptibilities, e.g. χ_π and χ_δ, can be easily deduced from the Wilson operator product expansion and dimensional arguments. The product of two dimension-three fermion bilinears separated by a space-time distance x should contain a constant behaving as $1/x^6$ as $x \to 0$. When integrated over space-time to form the susceptibility, this $1/x^6$ term will give a quadratic divergence. For the disconnected parts of the susceptibilities, a similar dimensional argument applies. However, the disconnected parts are constructed from the product of two independent fermion loops, each evaluated as a separate trace. For the case of scalar or pseudoscalar susceptibilities, chiral symmetry requires that each trace be proportional to m_l so the product will behave as m_l^2/x^4 leading to a logarithmic divergence multiplied by the very small factor m_l^2. Thus, if the continuum regulator respects chiral symmetry, then the $SU(2)_L \times SU(2)_R$ and $U(1)_A$-breaking differences $\chi_\pi - \chi_\sigma$, $\chi_\delta - \chi_\eta$, $\chi_\pi - \chi_\delta$ and $\chi_\eta - \chi_\sigma$ will all contain only small, logarithmic singularities proportional to $m_l^2 \ln(m_l/\Lambda)$ if evaluated in order-by-order in QCD perturbation theory, where Λ is the continuum cutoff scale.

In our lattice-regulated domain wall theory, the residual chiral symmetry breaking will result in these same differences containing small unphysical pieces of order $m_{\rm res}^2$. As in the case of the chiral condensate, $m_{\rm res}$ does not literally enter these differences but instead we expect that $m_{\rm res}^2$ will provide a reasonable estimate of their size. Note, when expressed in physical units $m_{\rm res} \sim e^{-\alpha L_s}/a$ so that our estimate $m_{\rm res}^2 \sim e^{-2\alpha L_s}/a^2$ of a chiral symmetry breaking difference remains quadratically divergent but is suppressed by the same factor that makes $m_{\rm res}$ small. (Here, for simplicity, we assume that the residual chiral symmetry breaking effects fall exponentially with increasing L_s, with an exponent α, unrelated to the α used earlier in this section.) For the purposes of this paper $m_{\rm res}^2 \sim (10 \text{ MeV})^2$, a quantity that is negligible on the $(\Lambda_{\rm QCD})^2 \approx (300 \text{ MeV})^2$ scale of the physical parts of the susceptibilities being subtracted.

Finally we examine two additional identities that hold in the continuum limit. The first is the relation between $\chi_{5,{\rm disc}}$ and the topological susceptibility $\chi_{\rm top}$. This relation begins with the identity

$$Q_{\rm top} = m_l^c \text{Tr}\left\{\gamma^5 \frac{1}{M_l}\right\}, \qquad (24)$$

which for the continuum theory will hold for each gauge configuration. Here for clarity we have introduced the quantity m_l^c to represent the light-quark mass in the continuum theory. This is easily understood by using a sum over Dirac operator eigenvectors to evaluate the trace and recognizing that the result is simply the number of right- minus the number of left-handed zero modes [20] which is equal to $Q_{\rm top}$ by the Atiyah-Singer theorem. Recall that

$$Q_{\rm top} = \frac{g^2}{32\pi^2} \int {\rm d}^4x F_{\mu\nu}^a(x)\tilde{F}_{\mu\nu}^a(x). \qquad (25)$$

Here $\tilde{F}_{\mu\nu} = \frac{1}{2}\sum_{\rho\sigma}\epsilon_{\mu\nu\rho\sigma}F_{\rho\sigma}$ where $\epsilon_{\mu\nu\rho\sigma}$ is the usual antisymmetric Levi-Civita tensor with $\epsilon_{1234} = 1$.

The desired identity:

$$\chi_{\rm top} = (m_l^c)^2 \chi_{5,{\rm disc}} \qquad (26)$$

is simply the ensemble average of the square of Eq. (24). This continuum equation should also relate DWF lattice quantities provided the total bare quark mass $\tilde{m}$ is used in place of the continuum mass m_l^c. As was explored at length in Ref. [9], this relation is badly violated for our lattice calculation because at our relatively coarse lattice spacing the quantity $Q_{\rm top}$ is difficult to compute directly. The right-hand side of Eq. (26) appears to nicely define the topological susceptibility giving the same answer even when the light-quark quantity $\tilde{m}_l^2 \chi_{5,{\rm disc}}$ is replaced with the corresponding strange quark quantity or the product of strange and light-quark expressions. [Note the right-hand side of Eq. (24) is expected to give the same result on a given gauge configuration independent of the quark mass.] For completeness $\chi_{5,{\rm disc}}/T^2$ and $\chi_{\rm top}/(\tilde{m}_l T_c)^2$ are tabulated in the two rightmost columns of Table III, where $\chi_{\rm top}$ is computed using the procedure described in Ref. [9]. As can be seen in Table III, their disagreement is substantial. However, the fractional discrepancy does decrease with increasing temperature (and decreasing lattice spacing) as should be expected if this is a finite lattice spacing artifact. We will not make further use of $\chi_{\rm top}$.

The second identity is the usual Ward identity connecting χ_π and the chiral condensate. This can be derived in the continuum for nonzero quark mass by evaluating the following integrated divergence:

$$0 = \int d^4x \partial_\mu \langle 0|T(A^{a\mu}(x)\pi^b(0))|0\rangle \qquad (27)$$

$$= \int d^4x \langle 0|T(-2m_l^c i\pi^a(x)\pi^b(0))|0\rangle - 2i\langle 0|\sigma(0)|0\rangle \delta^{ab}, \qquad (28)$$

where a and b are isospin indexes. Here the left term in the second line comes from the divergence of the axial current,

TABLE II.   The unrenormalized iso-vector pseudoscalar and mixed pseudoscalar/midpoint susceptibilities for the light and strange quarks as well as the combinations $(m_q\chi_\pi^q + \Delta_{\mathrm{mp}}^q)/T^3$ for $q = l, s$, which appear in the Ward identity, Eq. (31). The Ward identity requires the right and third-from-right columns to agree as well as agreement between the column second from the right above and the fifth column from the left in Table III. Moving from top to bottom, the three sections in this table correspond to the volumes $32^3 \times 8$, $24^3 \times 8$ and $16^3 \times 8$.

#	T(MeV)	β	χ_π^l/T^2	χ_π^s/T^2	$\Delta_{\mathrm{mp}}^l/T^3$	$\Delta_{\mathrm{mp}}^s/T^3$	$\frac{m_l\chi_\pi^l+\Delta_{\mathrm{mp}}^l}{T^3}$	$\frac{m_s\chi_\pi^s+\Delta_{\mathrm{mp}}^s}{T^3}$	Σ_l/T^3
1	139	1.633	313(2)	94.83(7)	13.34(8)	1.833(11)	9.94(6)	41.21(2)	10.07(4)
2	149	1.671	267(3)	93.15(7)	11.14(14)	1.939(10)	7.11(10)	36.52(3)	7.03(6)
3	159	1.707	214(3)	90.96(10)	4.77(7)	1.038(6)	5.71(9)	33.71(5)	5.80(6)
4	164	1.725	187(3)	89.57(12)	2.99(7)	0.757(5)	5.05(10)	32.00(5)	5.02(7)
5	168	1.740	161(3)	88.20(14)	1.91(6)	0.576(5)	4.16(11)	30.70(7)	4.16(8)
6	177	1.771	129(3)	85.64(11)	0.83(3)	0.329(2)	3.23(9)	27.94(3)	3.17(5)
7	186	1.801	100(2)	83.20(11)	0.33(1)	0.193(2)	2.39(6)	25.42(4)	2.46(4)
8	195	1.829	93(2)	80.81(9)	0.18(1)	0.118(1)	2.15(6)	23.20(2)	2.15(3)
9	149	1.671	270(13)	93.2(7)	11.6(7)	2.02(7)	7.5(5)	36.6(3)	7.10(6)
10	159	1.707	198(11)	90.6(6)	4.3(3)	1.05(4)	5.2(4)	33.6(3)	5.58(10)
11	168	1.740	164(8)	89.6(6)	1.96(15)	0.61(3)	4.3(3)	31.2(2)	4.40(10)
12	177	1.771	124(10)	85.7(5)	0.79(12)	0.33(2)	3.1(3)	28.0(2)	3.03(7)
13	186	1.801	99(3)	82.6(4)	0.31(2)	0.184(7)	2.35(8)	25.2(1)	2.58(6)
14	139	1.633	302(5)	95.0(2)	12.6(2)	1.825(21)	9.30(18)	41.26(8)	9.26(13)
15	149	1.671	247(5)	93.0(1)	10.1(2)	1.922(13)	6.34(14)	36.43(6)	6.26(12)
16	149	1.671	257(3)	93.6(1)	4.84(8)	0.815(7)	8.40(12)	38.24(6)	8.39(10)
17	159	1.707	189(5)	90.8(2)	4.09(16)	1.034(10)	4.92(19)	33.64(7)	5.25(17)
18	168	1.740	155(6)	88.3(2)	1.83(11)	0.573(7)	4.00(19)	30.73(8)	4.03(18)
19	177	1.771	127(7)	85.5(2)	0.80(7)	0.326(4)	3.15(19)	27.89(7)	3.16(15)
20	186	1.801	102(4)	83.5(2)	0.35(3)	0.196(3)	2.46(11)	25.50(6)	2.44(9)
21	195	1.829	91(2)	80.9(1)	0.17(1)	0.118(1)	2.10(5)	23.22(4)	2.10(5)

$\partial_\mu A(x)^{a\mu}$, while the right term results from the equal-time commutator that arises when the partial derivative with respect to the time is brought inside the time-ordered product. The result is the Gell-Mann-Oakes-Renner relation [21]:

$$m_l^c \chi_\pi = \Sigma_l. \qquad (29)$$

While this relation should be true in a continuum theory which has been regulated in a chirally symmetric way, both the right- and left-hand sides of Eq. (29) contain quadratic divergences as discussed earlier. Thus, we should not expect this equation to be obeyed in our DWF theory unless we take the limit of infinite L_s at finite a so that our theory has an exact chiral symmetry.

However, this equation has two important uses. First, we can repeat its derivation in our lattice theory using the partially conserved, five-dimensional axial current $\mathcal{A}^{a\mu}$ constructed by Furman and Shamir [22] and the divergence equation obeyed by $\mathcal{A}^{a\mu}$:

$$\partial_\mu \mathcal{A}^{a\mu} = -2im_l\pi^a + 2J_{5q}^a, \qquad (30)$$

where the definition of the "midpoint term" J_{5q}^a can be found in Ref. [23]. When used in the above derivation this relation yields the lattice identity:

$$2m_l\chi_\pi + \int d^4x \langle 0|T(iJ_{5q}(x)^a\pi^a(0))\rangle = 2\Sigma_l, \qquad (31)$$

for $a = 1, 2$ and 3. In the usual application of Eq. (30), iJ_{5q}^a is replaced in Eq. (31) by $m_{\mathrm{res}}\pi^a$ which would provide a DWF derivation of Eq. (29) in which the continuum light-quark mass m_l^c is replaced by $\tilde{m} = m_l + m_{\mathrm{res}}$. However, the low-energy relation $iJ_{5q}^a \approx m_{\mathrm{res}}\pi^a$ cannot be used here because short distances are involved. Nevertheless, we can simply evaluate both sides of Eq. (31) in our lattice calculation as a check of this discussion and find agreement within errors. Our numerical results for the three quantities which appear in Eq. (31) are tabulated in Table II for each of the seven temperatures studied as well as the right- and left-hand sides of Eq. (31) after a common factor of 2 has been removed. We also plot in Fig. 1 both the left- and right-hand sides of Eq. (31) as well $(m_l + m_{\mathrm{res}})\chi_\pi$, as the result of the naive use of the low-energy relation $iJ_{5q}^a \approx m_{\mathrm{res}}\pi^a$. The left panel of Fig. 1 shows these quantities for the light-quark case discussed here while the right panel shows the same quantities computed using the strange quark. In both Table II and Fig. 1, the mixed susceptibility appearing in Eq. (31) is represented by Δ_{mp}^f where

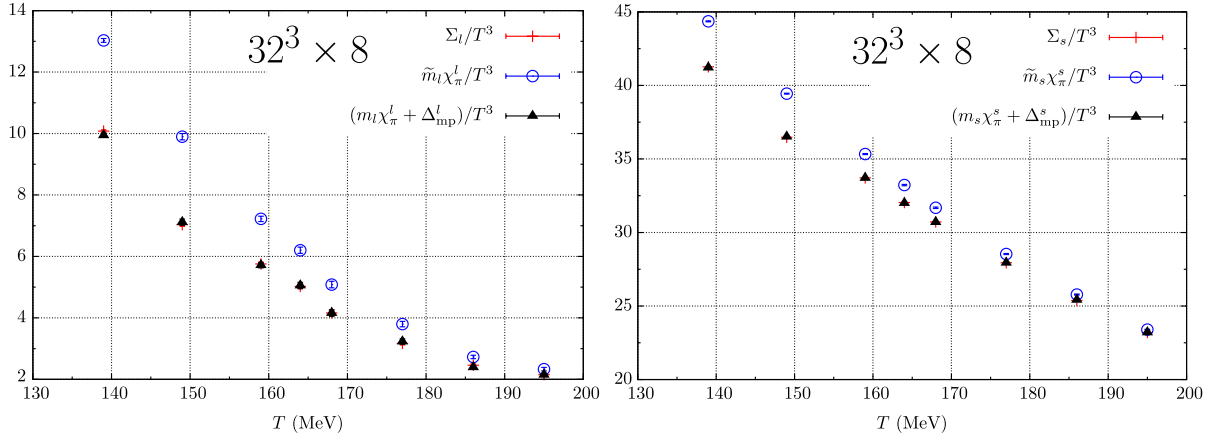$$\Delta_{\mathrm{mp}}^f = \int d^4x \langle 0|T(iJ_{5q}^{(f)}(x)\pi^{(f)}(0))\rangle, \qquad (32)$$

FIG. 1 (color online). The left panel shows the light-quark chiral condensate, Σ_l, and the sum of $m_l\chi_\pi$ and the mixed $\pi - J_{5q}/2$ susceptibility to which it should be equal according to the Ward identity in Eq. (31). Also shown is $(m_l + m_{\rm res})\chi_\pi \equiv \tilde{m}_l\chi_\pi$ which would equal Σ_l if $m_{\rm res}$ were the only effect of residual chiral symmetry breaking. The right panel shows the same quantities computed using the strange instead of the light quark. Similar agreement between the right- and left-hand sides of Eq. (31) is found for the 24^3 and 16^3 volumes, as can be seen from Table II.

where in this equation we construct the quark bilinears $J_{5q}^{(f)}$ and $\pi^{(f)}$ from a single flavor of quark specified by $f = l$ or s and include only connected graphs, in which the quark fields are contracted between J_{5q} and π. In these tables and figures and those which follow, when a combination of quantities that were computed separately are combined, such as $m_l\chi_\pi^l + \Delta_{\rm mp}^l$, we will use the jackknife method with data that has been averaged over bins of 50 configurations to compute the error on the combined quantity so that the effects of statistical correlations between the quantities being combined are included. However, for simplicity, if a computed renormalization factor, factor of a expressed in physical units or factor of $m_{\rm res}$ appears, these factors usually have smaller errors than the quantities they multiply and their fluctuations will be ignored.

A second use of Eq. (29) is to provide a method to compute a more physical result for $\Delta_{l,s}$ in a DWF calculation. Since no chiral limit has been taken in the continuum derivation of Eq. (29), it will hold equally well if applied to either strange or light quarks. If we use the resulting equations for Σ_l and Σ_s to determine the weighted difference $\Delta_{l,s}$ we obtain

$$\Delta_{l,s} = m_l^c(\chi_{\pi_l} - \chi_{\pi_s}), \tag{33}$$

where we use the symbol χ_{π_s} to represent the "pion" susceptibility that results if the light-quark mass is replaced by that of the strange quark and add the subscript l to the usual pion susceptibility for clarity. From the perspective of the continuum theory both sides of Eq. (33) provide an equally good value for the subtracted chiral condensate. Neither quantity contains a quadratic divergence and the much smaller logarithmic divergences present on both sides are equal. For a DWF theory with residual chiral symmetry breaking this equation does not hold and the left-hand side

$\Delta_{l,s}$ contains an unphysical additive constant $O(m_{\rm res}/a^2)$. However, the right-hand side is much better defined with no $1/a^2$ term. Thus, we can use the right-hand side of Eq. (33) to provide a more physical result for $\Delta_{l,s}$ which will contain only a small, unphysical piece of order $m_l m_s^2 \ln(m_s a)$. Thus, we can define an improved value for $\Delta_{l,s}$:

$$\tilde{\Delta}_{l,s} = \tilde{m}_l(\chi_{\pi_l} - \chi_{\pi_s}), \tag{34}$$

which we will use to compare with spectral formulas and with the results for $\Delta_{l,s}$ from other lattice fermion formulations.

B. Chiral symmetry restoration

In this section we present and discuss our numerical results for the chiral condensate and for the disconnected chiral susceptibility as a function of temperature. Figure 2 shows the Monte Carlo time histories of the light-quark chiral condensate for seven of the temperatures studied. The time evolutions for the $32^3 \times 8$ ensembles are displayed in the left panel and those from $24^3 \times 8$ in the right. The evolutions of the light-quark condensates from both sets of ensembles appear to follow the same trend. For the lower temperature region ($T \leq 168$ MeV), the light-quark condensate fluctuates around its average value. However, as temperature grows higher, the fluctuations can better be described as upward spikes added to an otherwise flat base line.

This behavior is typically seen in finite-temperature DWF calculations and arises because above T_c the main contribution to the chiral condensate comes from isolated, near-zero modes [24]. These modes become increasingly infrequent as the temperature is increased but, when present, produce a noisy, nonzero chiral condensate. The noise results from the relatively small space-time extent of
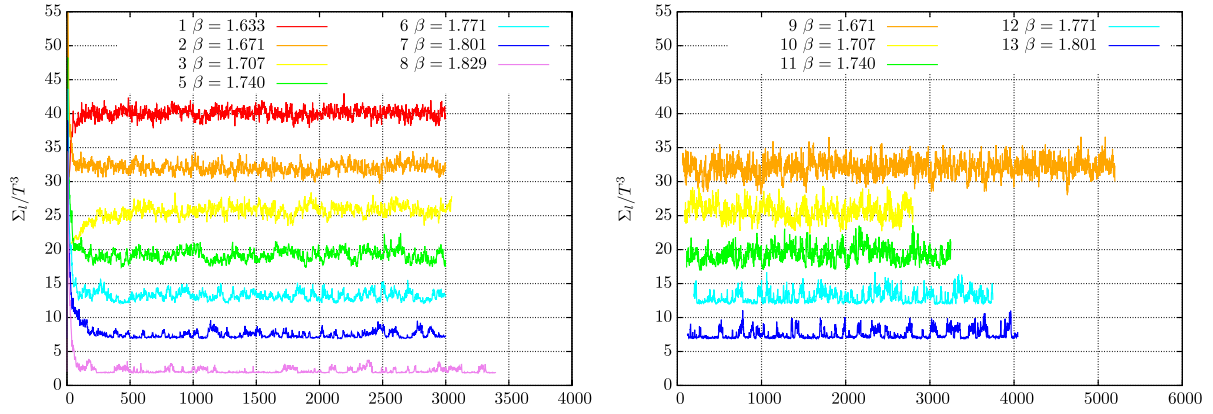
FIG. 2 (color online).   Monte Carlo time histories of the light-quark chiral condensate Σ_l/T^3 on the $32^3 \times 8$ (left) and $24^3 \times 8$ (right) ensembles. (Only the longest streams from run #9 and #10 are displayed.) There is a vertical offset of 5 units between successive data sets with the $\beta = 1.829$ results unshifted. Note that the time evolution corresponding to $\beta = 1.725$, $32^3 \times 8$ (run #4) behaves in a similar manner to those of its neighboring ensembles, but is omitted from the graph to preserve a uniform separation between each ensemble.

each zero mode which is therefore sampled in our stochastic determination with relatively few random numbers.

Such behavior becomes most pronounced for $T \geq 186$ MeV in the $32^3 \times 8$ calculations. At $T = 177$ MeV, the $24^3 \times 8$ Monte Carlo time evolution shows this characteristic plateau-spike structure more distinctly than does the comparable $32^3 \times 8$ time history. This suggests a lower pseudocritical transition temperature for the smaller volume or that the larger 32^3 volume supports a larger number of such zero modes, reducing the size of the intervals when none are present and the chiral condensate is nearly zero.

The ensemble averages of the light, subtracted and strange chiral condensates are summarized in Table III. The temperature dependence of the light and the subtracted condensates is also illustrated in Fig. 3. As that figure shows, results from $32^3 \times 8$ and $24^3 \times 8$ ensembles agree well throughout the transition region, whereas those from the $16^3 \times 8$ ensembles show an appreciable discrepancy for $T < 168$ MeV, indicating a small but well-resolved finite-volume effect.

A second measure of the restoration of $SU(2)_L \times SU(2)_R$ symmetry is the two differences $\chi_\pi - \chi_\sigma$ and

TABLE III.   The unrenormalized chiral condensates and disconnected chiral susceptibilities. The two rightmost columns should agree according to Eq. (26). As discussed, we attribute their large difference to inaccuracy in the strong-coupling measurement of χ_{top}. Moving from top to bottom, the three sections correspond to the volumes $32^3 \times 8$, $24^3 \times 8$ and $16^3 \times 8$.

| #	T (MeV)	β	Σ_l/T^3	Σ_s/T^3	$\Delta_{l,s}/T^3$	χ_{disc}/T^2	$\chi_{5,\text{disc}}/T^2$	$\chi_{\text{top}}/(\tilde{m}_l T)^2$
1	139	1.633	10.07(4)	41.27(2)	6.40(4)	20(2)	118(7)	261(11)
2	149	1.671	7.03(6)	36.48(2)	3.84(5)	28(3)	94(8)	177(11)
3	159	1.707	5.80(6)	33.73(2)	2.83(6)	33(3)	70(8)	118(10)
4	164	1.725	5.02(7)	32.04(3)	2.16(7)	38(3)	49(4)	78(4)
5	168	1.740	4.16(8)	30.72(3)	1.46(7)	37(3)	38(5)	54(4)
6	177	1.771	3.17(5)	27.94(2)	0.71(5)	22(2)	24(3)	37(3)
7	186	1.801	2.46(4)	25.38(2)	0.22(4)	12(2)	10(2)	15(2)
8	195	1.829	2.15(3)	23.20(1)	0.14(3)	7(1)	10(1)	15(2)
9	148	1.671	7.10(6)	36.53(2)	3.90(6)	31(2)	89(5)	165(7)
10	159	1.707	5.58(10)	33.68(3)	2.66(10)	36(3)	64(6)	110(6)
11	168	1.740	4.40(10)	30.84(4)	1.69(10)	32(3)	47(6)	67(6)
12	177	1.771	3.03(7)	27.90(3)	0.57(7)	19(2)	21(3)	32(3)
13	186	1.801	2.58(6)	25.41(2)	0.34(6)	13(2)	14(2)	18(2)
14	139	1.633	9.26(13)	41.02(4)	5.61(12)	36(3)	113(7)	252(11)
15	149	1.671	6.26(12)	36.42(5)	3.07(12)	44(3)	89(6)	159(6)
16	149	1.671	8.39(10)	38.30(3)	5.00(10)	41(2)	90(6)	168(7)
17	159	1.707	5.25(17)	33.81(6)	2.27(16)	43(4)	55(6)	97(7)
18	168	1.740	4.03(18)	30.66(7)	1.33(18)	35(5)	37(5)	60(7)
19	177	1.771	3.16(15)	27.88(6)	0.71(15)	25(4)	24(4)	36(4)
20	186	1.801	2.44(9)	25.43(4)	0.20(9)	11(4)	9(3)	21(6)
21	195	1.829	2.10(5)	23.22(3)	0.09(5)	6(2)	6(2)	11(2)
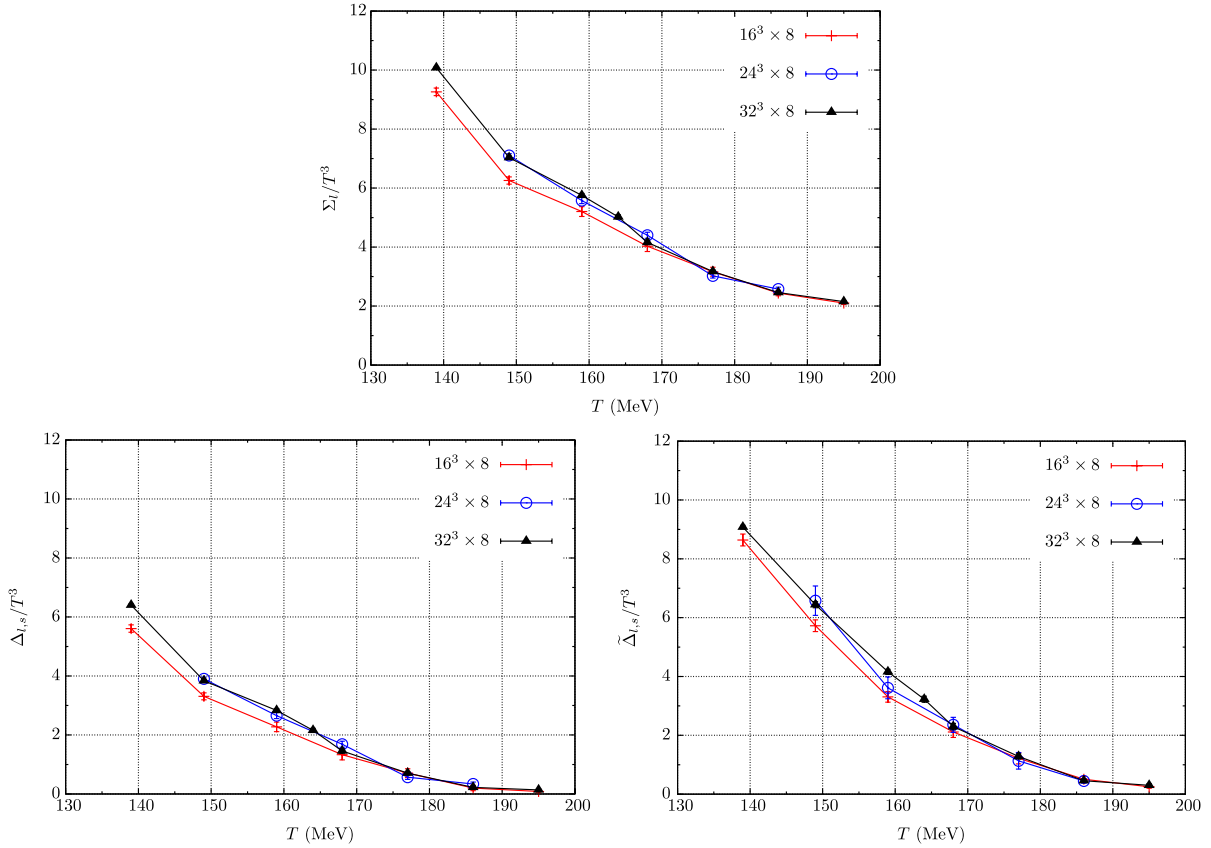
FIG. 3 (color online).   Comparison of light-quark (upper), subtracted (lower left) and improved subtracted (lower right) chiral condensates computed on different volumes. The 32^3 and 24^3 volumes agree reasonably well for all temperatures but are 5%–10% larger than the corresponding values from the 16^3 volume for $T < 168$ MeV. The results appear to be volume independent for $T \geq 168$ MeV.

$\chi_\eta - \chi_\delta$, following Eq. (13). These two $SU(2)_L \times SU(2)_R$-breaking differences are plotted in Fig. 4. The quantity $\chi_\pi - \chi_\sigma$ shows the behavior that might be expected from the temperature dependence of the chiral condensate shown in Fig. 3. A large $SU(2)_L \times SU(2)_R$-breaking difference is seen for $T \leq 159$ MeV which becomes zero for $T \geq 168$ MeV. The second difference $\chi_\eta - \chi_\delta$ is more surprising, being essentially zero throughout our temperature range. While we do not have a crisp explanation for this unexpected $SU(2)_L \times SU(2)_R$ symmetry below T_c we do expect this difference to vanish for $T > T_c$ and to be small relative to $\chi_\pi - \chi_\sigma$ for $T < T_c$ since the large value of χ_π reflects the small pion mass while the δ, σ and η are all expected to be relatively massive below T_c.

While the chiral condensate is the order parameter for the chiral transition, its strong apparent temperature dependence results from a combination of the finite-temperature physics of interest and its dependence on the lattice scale as a dimension-three operator. (This can be recognized by noting that we often discuss the dimensionless quantity Σ_l/T^3 which will change significantly with temperature simply because of the $1/T^3$ factor.) The location of the pseudocritical temperature is much more easily seen by examining the disconnected chiral susceptibility χ_{disc}. This

has dimension 2 and so varies a little less strongly with the lattice scale (which we are changing to vary T on our $N_\tau = 8$ lattice) and shows a dramatic peak near the transition which can be used to define the location of the pseudocritical temperature T_c. Numerical results for χ_{disc} before renormalization are presented in Table III. In order to allow a comparison with results from the staggered formalism, the susceptibilities should be normalized in the $\overline{\mathrm{MS}}$ scheme at 2 GeV. They can be obtained from the directly computed lattice quantities using the relation:

$$\chi^{\overline{\mathrm{MS}}} = \left(\frac{1}{Z_{m_f \to \overline{\mathrm{MS}}}} \right)^2 \chi^{\mathrm{bare}}. \tag{35}$$

The renormalization factors $Z_{m_f \to \overline{\mathrm{MS}}}$ for each temperature are listed in Table IV. These values for $Z_{m_f \to \overline{\mathrm{MS}}}$ were obtained in Ref. [9] from the dependence of the pion mass, expressed in physical units, on the input quark mass and the known value of $\tilde{m}_l$ which corresponds to the physical value of m_π [25].

The dependence of the renormalized χ_{disc} on volume is shown in the left panel of Fig. 5. At $T = 168$ MeV and above the disconnected chiral susceptibilities from all volumes agree within errors. However, at lower
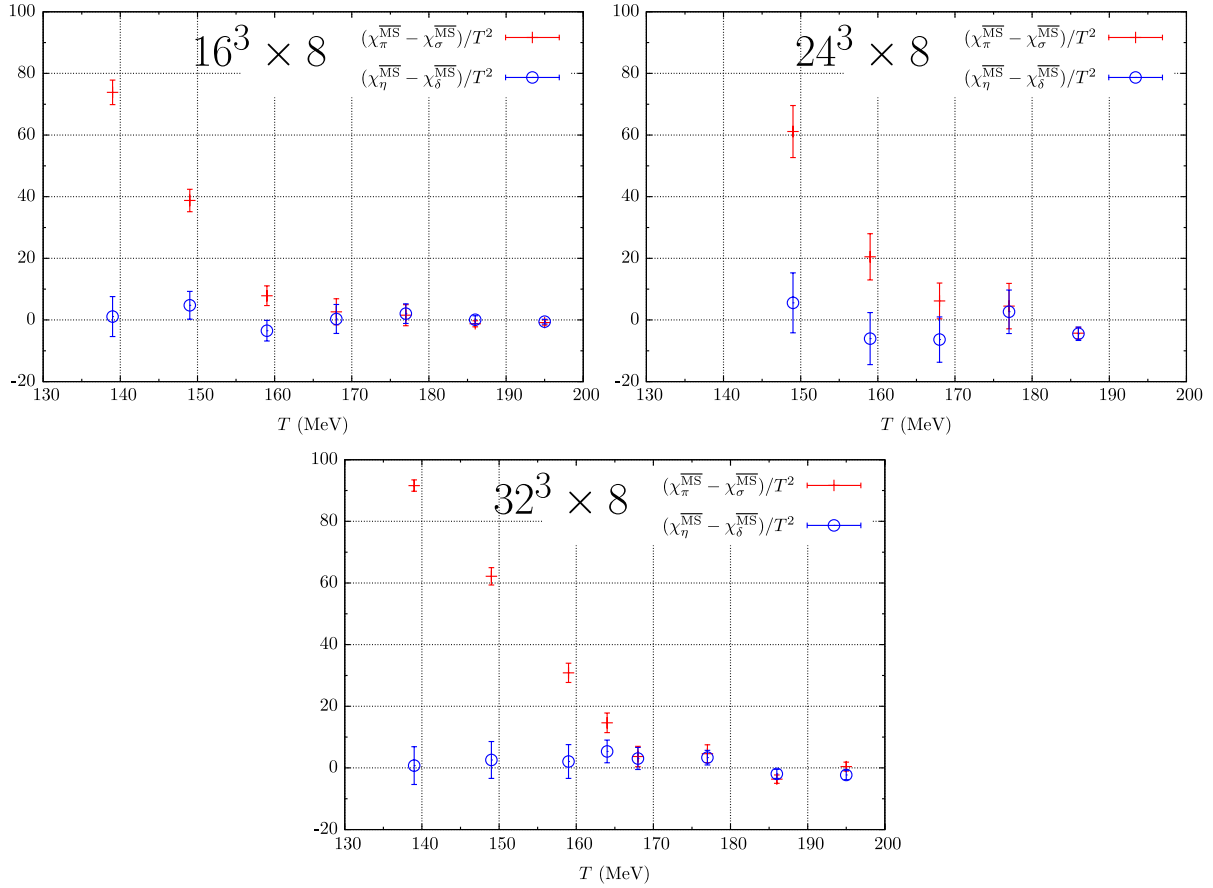
FIG. 4 (color online).   The two $SU(2)_L \times SU(2)_R$-breaking susceptibility differences $\chi_\pi^{\overline{MS}} - \chi_\sigma^{\overline{MS}}$ and $\chi_\delta^{\overline{MS}} - \chi_\eta^{\overline{MS}}$ plotted as a function of temperature for our three spatial volumes: 16^3, 24^3 and 32^3. For temperatures of 170 MeV and above these differences are consistent with zero and the expected restoration of chiral symmetry above T_c. The quantity $\chi_\pi - \chi_\sigma$ becomes very large below T_c reflecting the small mass of the pseudo-Goldstone π meson below T_c. In contrast, the second difference $\chi_\eta - \chi_\delta$ remains relatively small as the temperature decreases below T_c, reflecting the relatively large masses of the δ and η mesons.

temperatures there is a large discrepancy between the $16^3 \times 8$ and the $32^3 \times 8$ ensembles which becomes larger as temperature decreases. Results from $24^3 \times 8$, fall in between, although they tend to lie closer to the $32^3 \times 8$ points.

Since we are studying only a single value of N_τ and a pion mass that is larger than physical by a factor of 1.5, it is premature to draw a definite quantitative conclusion about the pseudocritical transition temperature. However, a qualitative examination of the left panel in Fig. 5 suggests that a peak in χ_{disc} occurs for the 16^3 and 24^3 volumes at approximately 160 MeV and that this peak position increases to slightly above 165 MeV as the volume is increased to 32^3.

The right panel of Fig. 5 compares the $m_\pi = 200$ MeV, $32^3 \times 8$ DWF results for χ_{disc} with those obtained from staggered fermions using a $48^3 \times 12$ volume and the highly improved staggered quark (HISQ) and a-squared tadpole improved (ASQTAD) staggered actions with $m_\pi = 161$ and 177 MeV respectively [26]. Again, the disconnected chiral condensates are consistent among these three methods for $T \geq 175$ MeV. However, the ASQTAD results lie

substantially below the DWF and HISQ results for temperatures at and below the transition region. The HISQ results are in good agreement with the $32^3 \times 8$ DWF results. However, this agreement appears to be coincidental, since the HISQ results are obtained for a quoted pion mass of 161 MeV, significantly smaller than the 200 MeV pion mass of the DWF ensembles. The expected strong dependence of χ_{disc} near T_c on the pion mass suggests that $m_\pi = 160$ MeV DWF results would lie above those found with HISQ. The discrepancy between the DWF and ASQTAD results and the expected discrepancy with comparable HISQ results are likely explained by lattice discretization errors associated with staggered taste symmetry breaking.

C. $U(1)_A$ symmetry

We will now discuss the degree to which the anomalous $U(1)_A$ symmetry is restored above T_c by examining the two implications of this symmetry for the four susceptibilities given in Eq. (14): $\chi_\pi = \chi_\delta$ and $\chi_\sigma = \chi_\eta$. The numerical results for each of these four susceptibilities are

TABLE IV.   Results for the four independent susceptibilities $\chi_\pi, \chi_\delta, \chi_\sigma$ and χ_η as well as the two pairs of differences, $\Delta_{\pi,\sigma} = \chi_\pi - \chi_\sigma$, $\Delta_{\eta,\delta} = \chi_\eta - \chi_\delta$ and $\Delta_{\pi,\delta} = \chi_\pi - \chi_\delta$, $\Delta_{\sigma,\eta} = \chi_\sigma - \chi_\eta$ which measure the degree of $SU(2)_L \times SU(2)_R$ and $U(1)_A$ symmetry, respectively. All of these susceptibilities are renormalized in the $\overline{\rm MS}(\mu = 2 \text{ GeV})$ scheme using the renormalization factor listed in the $Z_{m_f \to \overline{\rm MS}}$ column. Moving from top to bottom, the three sections correspond to the volumes $32^3 \times 8$, $24^3 \times 8$ and $16^3 \times 8$.

#	T (MeV)	$Z_{m_f \to \overline{\rm MS}}$	$\chi_\pi^{\overline{\rm MS}}/T^2$	$\chi_\delta^{\overline{\rm MS}}/T^2$	$\chi_\sigma^{\overline{\rm MS}}/T^2$	$\chi_\eta^{\overline{\rm MS}}/T^2$	$\Delta_{\pi,\sigma}^{\overline{\rm MS}}/T^2$	$\Delta_{\eta,\delta}^{\overline{\rm MS}}/T^2$	$\Delta_{\pi,\delta}^{\overline{\rm MS}}/T^2$	$\Delta_{\sigma,\eta}^{\overline{\rm MS}}/T^2$
1	139	1.47	144.7(7)	34.0(3)	53(2)	35(6)	92(2)	1(6)	111(1)	18(6)
2	149	1.49	120.1(1.3)	33.1(6)	58(2)	36(6)	62(3)	3(6)	87(2)	22(7)
3	159	1.51	94.0(1.1)	34.3(5)	63(3)	36(6)	31(3)	2(5)	60(2)	27(6)
4	164	1.52	80.8(1.3)	33.2(8)	66(3)	39(4)	15(3)	5(4)	48(2)	28(5)
5	168	1.53	68.7(1.4)	33.6(9)	65(3)	37(4)	4(3)	3(4)	35(2)	28(4)
6	177	1.55	53.8(1.3)	30.8(1.1)	49(2)	34(2)	5(3)	3(2)	23(2)	15(3)
7	186	1.57	40.6(8)	34.1(6)	44(1)	32(1)	−4(1)	−2(1)	6(1)	12(2)
8	195	1.58	37.2(9)	31.1(8)	37(1)	29(1)	0.4(1.4)	−2(2)	6(2)	8(2)
9	149	1.49	122(6)	32(2)	61(4)	38(9)	61(8)	6(10)	90(8)	23(10)
10	159	1.51	87(5)	37(2)	66(4)	31(7)	20(8)	−6(8)	50(6)	35(10)
11	168	1.53	70(3)	36(2)	64(3)	30(7)	6(6)	−6(7)	34(5)	34(9)
12	177	1.55	52(4)	31(3)	47(4)	34(4)	4(7)	3(7)	20(7)	13(8)
13	186	1.57	40(1)	34(1)	44(1)	29(2)	−4(2)	−4(2)	7(2)	15(3)
14	139	1.47	140(2)	33(2)	66(3)	34(7)	74(4)	1(6)	107(4)	32(8)
15	149	1.49	111(2)	33(2)	73(2)	38(6)	39(4)	5(5)	78(4)	35(7)
17	159	1.51	83(2)	38(2)	75(3)	35(4)	8(3)	−3(3)	45(4)	40(6)
18	168	1.53	66(3)	33(2)	64(4)	34(5)	3(4)	0.3(4.7)	33(4)	30(9)
19	177	1.55	53(3)	31(2)	51(2)	33(3)	2(3)	2(3)	22(5)	19(5)
20	186	1.57	41(1)	34(1)	43(2)	34(2)	−1(1)	0.1(1.3)	8(3)	9(4)
21	195	1.58	36(1)	32(1)	37(1)	31(1)	−1(1)	−0.5(8)	5(2)	6(2)

summarized in Table IV as well as their $U(1)_A$-breaking differences $\chi_\pi - \chi_\delta$ and $\chi_\sigma - \chi_\eta$ which we will often abbreviate as $\Delta_{\pi,\delta} = \chi_\pi - \chi_\delta$ and $\Delta_{\sigma,\eta} = \chi_\sigma - \chi_\eta$. The integrated susceptibilities χ_π and χ_δ are calculated from the corresponding two point correlation functions by summing the position of the sink over the entire space-time volume. For the $24^3 \times 8$ ensembles, we use a single point source located at $(0, 0, 0, 0)$, while for the $16^3 \times 8$ and $32^3 \times 8$ ensembles, we use a random Z_2 wall source located on a fixed, three-dimensional spatial slice, $x_z = 0$.

These two $U(1)_A$-breaking differences are plotted in Fig. 6. As can be seen, these diminish rapidly with temperature but are many standard deviations from zero even at the temperatures of 177 and 186 MeV, well above T_c. We expect that the effect of explicit chiral symmetry breaking, either from the nonzero input quark mass or finite L_s, residual chiral symmetry breaking, on these differences will be much smaller. Specifically, for $T > T_c$ we might estimate the contribution of explicit $U(1)_A$ breaking to be of order $\tilde{m}_l^2/T^2 \sim (0.004 * 8)^2 = 0.001$ compared to
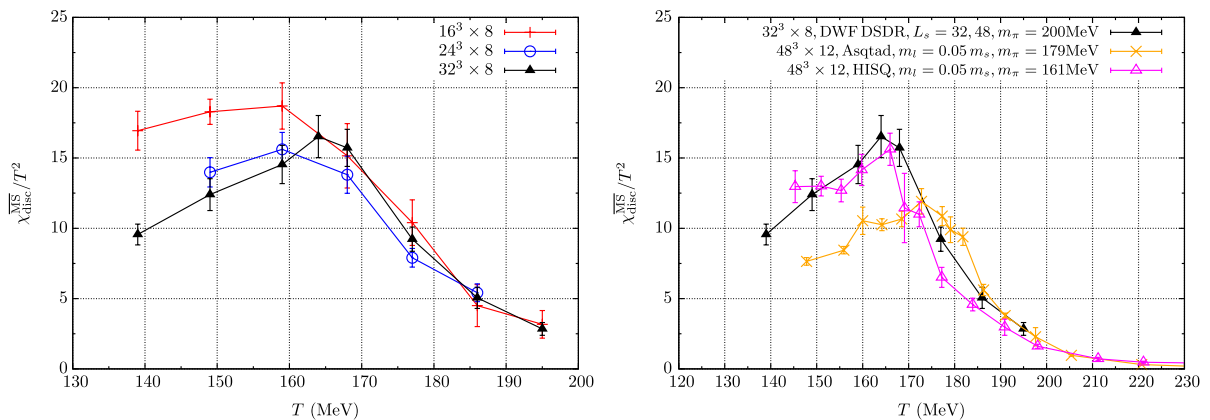

FIG. 5 (color online).   The left panel compares $\chi_{\rm disc}$ computed using DWF on 32^3, 24^3 and 16^3 volumes. Significant volume dependence can be seen between 32^3 and 16^3, while the 24^3 results agree with those from 32^3 within errors. The right panel compares the 32^3, $N_\tau = 8$ DWF results for $\chi_{\rm disc}$ with those from staggered fermions on a $48^3 \times 12$ volume using both the ASQTAD and HISQ actions [26]. In each case $\chi_{\rm disc}$ is renormalized in the $\overline{\rm MS}(\mu = 2 \text{ GeV})$ scheme.
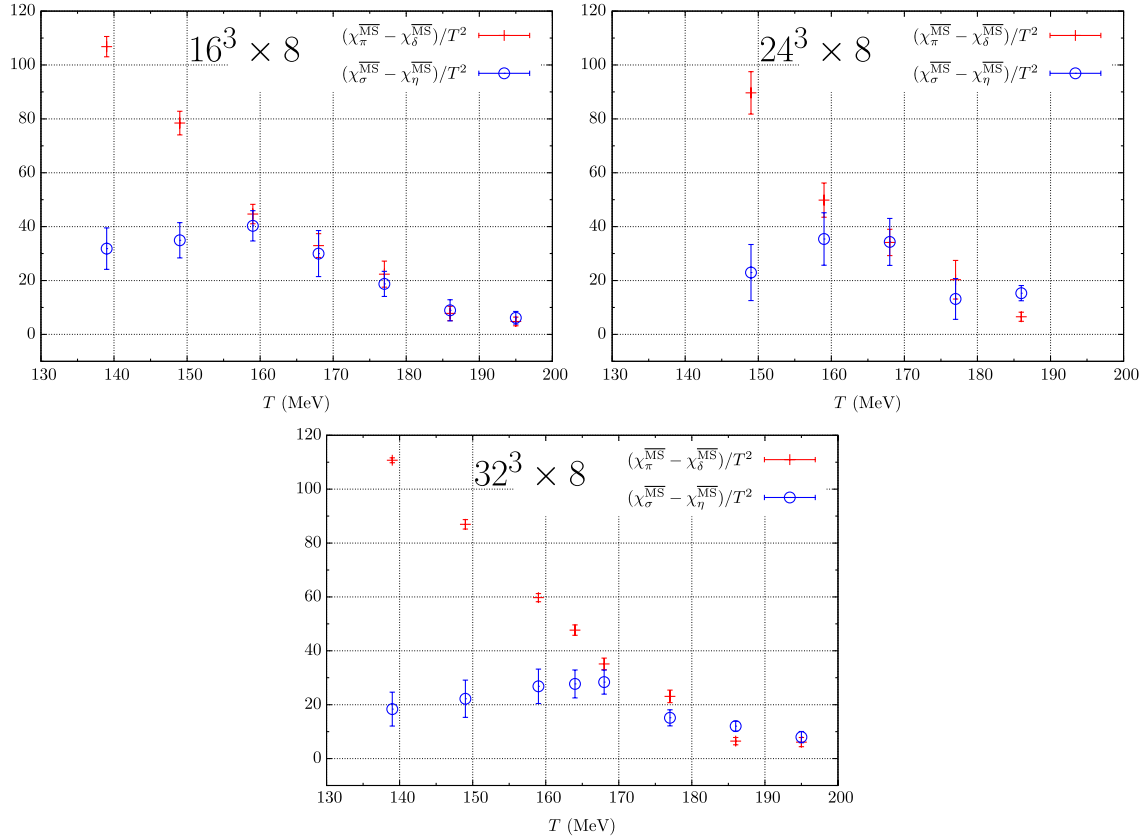
FIG. 6 (color online). The two $U(1)_A$-violating susceptibility differences, $\chi_\pi^{\overline{\text{MS}}} - \chi_\delta^{\overline{\text{MS}}}$ and $\chi_\sigma^{\overline{\text{MS}}} - \chi_\eta^{\overline{\text{MS}}}$ plotted as a function of temperature for our three spatial volumes. As expected these quantities are very different below T_c. However, even for temperatures of 160 MeV and above these quantities differ from zero by many standard deviations, providing clear evidence for anomalous symmetry breaking above T_c. The near equality of these two differences above T_c, which are related by $SU(2)_L \times SU(2)_R$ symmetry suggests that the effects of explicit chiral symmetry breaking are much smaller (as expected) than this anomalous symmetry breaking.

results between 3 and 7 shown in Table IV.[1] Numerical evidence for the absence of explicit chiral symmetry breaking is provided by the near equality of the two differences $\chi_\pi - \chi_\delta$ and $\chi_\sigma - \chi_\eta$ which are related by $SU(2)_L \times SU(2)_R$ symmetry, a symmetry also explicitly broken by m_l and m_{res}.

Strong evidence for the small size of possible explicit chiral symmetry breaking also comes from the results for $\chi_\pi - \chi_\delta$ computed for the strange quark. It is the explicit breaking of chiral symmetry by the valence propagators which can create a nonanomalous signal for $\chi_\pi - \chi_\delta$. As can be seen from Table V the results for $\chi_\pi - \chi_\delta$ are smaller for the strange than for the light quark. If the strange quark results are interpreted as coming entirely from explicit chiral symmetry breaking, the corresponding effects for the light quarks should be reduced by a factor of

$(\tilde{m}_l/\tilde{m}_s)^2 \approx 0.008$. At $T = 179$ MeV, this approach gives explicit chiral symmetry breaking for the light-quark quantity $\chi_\pi - \chi_\delta$ of order $4.26 \cdot 0.008 = 0.034$. This is larger than the 0.001 estimate above but only a fraction of a percent of the signal. Thus, we interpret the results for $\chi_\pi - \chi_\delta$ and $\chi_\sigma - \chi_\eta$ shown in Table IV and Fig. 6 as clear evidence for the anomalous breaking of $U(1)_A$ symmetry for $T > T_c$.

IV. LOW-LYING EIGENVALUE SPECTRUM

In Sec. III we studied the QCD transition region by examining the temperature dependence of vacuum expectation values and correlation functions whose behavior is closely related to the $SU(2)_L \times SU(2)_R$ and $U(1)_A$ symmetries that are restored, or partially restored, as the temperature is increased through the transition region. In this section we will examine a different quantity, the spectrum of the light-quark Dirac operator, which is also directly related to the violation of these symmetries. In the first subsection, Sec. IV A, we review the basic formulas relating the Dirac eigenvalue spectrum to other measures of $SU(2)_L \times SU(2)_R$ and $U(1)_A$ symmetry breaking in

---

[1]This assumed quadratic dependence on $\tilde{m}_l$ does not allow for a possible combined effect of explicit chiral symmetry breaking and the sort of nonanalytic behavior above T_c that we are trying to study. We do not have sufficient numerical results to study such effects which we view as "second order" since they require both nonperturbative chiral breaking above T_c and $\tilde{m}_l \neq 0$.

TABLE V.   The same quantities as tabulated in Table IV but with the light quark replaced by the strange quark.

#	T (MeV)	$\chi_\pi^{s,\overline{\mathrm{MS}}}/T^2$	$\chi_\delta^{s,\overline{\mathrm{MS}}}/T^2$	$\chi_\sigma^{s,\overline{\mathrm{MS}}}/T^2$	$\chi_\eta^{s,\overline{\mathrm{MS}}}/T^2$	$\Delta_{\pi,\sigma}^{s,\overline{\mathrm{MS}}}/T^2$	$\Delta_{\eta,\delta}^{s,\overline{\mathrm{MS}}}/T^2$	$\Delta_{\pi,\delta}^{s,\overline{\mathrm{MS}}}/T^2$	$\Delta_{\sigma,\eta}^{s,\overline{\mathrm{MS}}}/T^2$
1	139	43.89(3)	31.50(2)	33.7(2)	42.9(4)	10.1(2)	11.4(4)	12.39(5)	−9.2(4)
2	149	41.96(3)	31.70(3)	33.8(2)	41.6(3)	8.2(2)	9.9(3)	10.26(5)	−7.9(4)
3	159	39.89(4)	31.71(3)	34.8(4)	39.0(3)	5.1(4)	7.3(3)	8.18(7)	−4.2(4)
4	164	38.77(5)	31.74(4)	35.6(4)	38.1(4)	3.2(4)	6.4(4)	7.02(8)	−2.6(5)
5	168	37.68(6)	31.67(3)	35.3(4)	37.1(3)	2.4(4)	5.4(3)	6.00(9)	−1.8(5)
6	177	35.65(5)	31.39(2)	33.4(3)	35.1(3)	2.2(3)	3.7(4)	4.26(6)	−1.7(5)
7	186	33.75(5)	30.83(3)	32.7(3)	33.4(3)	1.1(3)	2.5(3)	2.93(6)	−0.7(3)
8	195	32.37(4)	30.46(2)	31.7(1)	32.2(2)	0.7(1)	1.7(2)	1.91(4)	−0.5(3)
9	149	42.0(3)	31.57(16)	34.0(5)	41.5(5)	7.9(6)	10.0(5)	10.4(4)	−7.5(7)
10	159	39.7(3)	31.82(12)	34.4(3)	39.0(5)	5.3(4)	7.2(6)	7.9(4)	−4.6(6)
11	168	38.3(3)	31.73(11)	33.9(4)	37.7(4)	4.3(6)	5.9(4)	6.5(3)	−3.7(6)
12	177	35.7(2)	31.45(9)	33.5(2)	35.5(4)	2.2(3)	4.1(4)	4.2(3)	−2.0(5)
13	186	33.5(1)	30.84(7)	32.3(2)	32.9(3)	1.2(2)	2.0(3)	2.7(2)	−0.6(4)
14	139	43.95(7)	31.52(5)	33.8(2)	43.6(3)	10.2(2)	11.5(3)	12.44(11)	−9.3(4)
15	149	41.87(6)	31.79(5)	34.8(3)	41.1(4)	7.1(3)	9.4(4)	10.08(9)	−6.4(5)
17	159	39.81(8)	31.72(6)	34.6(3)	39.7(3)	5.2(3)	8.0(3)	8.09(13)	−5.1(4)
18	168	37.72(10)	31.68(6)	34.7(4)	38.0(4)	3.0(4)	6.4(4)	6.04(14)	−3.3(5)
19	177	35.58(9)	31.41(6)	33.9(2)	35.6(3)	1.6(2)	4.2(3)	4.18(13)	−1.7(3)
20	186	33.86(8)	30.87(4)	32.7(1)	34.0(2)	1.2(2)	3.1(2)	2.99(10)	−1.3(3)
21	195	32.41(6)	30.48(3)	31.8(1)	32.2(3)	0.6(1)	1.7(3)	1.92(5)	−0.3(3)

continuum field theory. In Sec. IV B we present the distribution found for the 100 lowest Dirac eigenvalues for each of the six temperatures studied between 150–200 MeV on our largest, $32^3 \times 8$ volume. Finally in Secs. IV C and IV D we make a quantitative connection between this measured eigenvalue spectrum and the subtracted chiral condensate $\Delta_{l,s}$ and the $U(1)_A$-breaking susceptibility difference $\Delta_{\pi,\delta} = \chi_\pi - \chi_\delta$, respectively. As is discussed in Sec. IV D, at temperatures just above T_c the Dirac spectrum agrees well with the predictions of the dilute instanton gas approximation and this approximation provides a good quantitative description of the anomalous $U(1)_A$ symmetry breaking difference $\chi_\pi - \chi_\delta$ seen in this region.

A. Preliminaries

The most familiar relation between the Dirac spectrum and an important QCD observable is the spectral expression for the chiral condensate,

$$\Sigma_q = -\langle \bar{\psi}\psi \rangle_q = \int_0^\infty d\lambda \rho(\tilde{m}_l, \tilde{m}_s, \lambda) \frac{2\tilde{m}_q}{\tilde{m}_q^2 + \lambda^2}, \quad q = l, s.$$

$$(36)$$

Here we have used the symmetry $\rho(\lambda) = \rho(-\lambda)$, limiting the integral to non-negative values of λ and introducing the compensating factor of 2 in the numerator. In the infinite volume and chiral limits and applied to the light-quark condensate, this equation becomes the well-known Banks-Casher relation [27]:

$$-\lim_{\tilde{m}_l \to 0} \lim_{V \to \infty} \langle \bar{\psi}\psi \rangle_l = \lim_{\lambda \to 0} \lim_{\tilde{m}_l \to 0} \lim_{V \to \infty} \pi\rho(\tilde{m}_l, \tilde{m}_s, \lambda). \quad (37)$$

Therefore, if the eigenvalue density $\rho(\tilde{m}, \lambda)$ is nonvanishing in infinite volume at the origin, chiral symmetry will be broken by a nonvanishing quark condensate.

While we have used the lattice variable $\tilde{m}_q$ to represent the quark mass in this equation, it should be emphasized that this is an equation derived in continuum field theory. The equivalent expression, derived for DWF in a lattice theory will be quite different. For example, a spectral expression for Σ_q derived from an eigenmode expansion of the DWF lattice propagator will involve wave functions for the five-dimensional modes evaluated on and integrated over the two $s = 0$ and $s = L_s - 1$, four-dimensional faces, yielding an expression significantly more complex than that given in Eq. (36) [23]. However, when appropriately renormalized, the eigenvalue density $\rho(\tilde{m}, \lambda)$ is a physical quantity that can be computed using lattice methods [28]. Thus, as in Ref. [9], we compute the low-lying spectrum $\rho^{\text{latt}}(\lambda)$ of the Hermitian DWF Dirac operator, $D_H = \gamma^5 R_5 D_{\text{DWF}}$, where R_5 is the reflection operator in the fifth dimension: $s \to L_s - 1 - s$ for the fifth-dimension coordinate $0 \leq s \leq L_s - 1$. We then use the β-dependent renormalization factor $Z_{\text{tw} \to \overline{\mathrm{MS}}}$ to transform $\rho^{\text{latt}}(\lambda)$ into $\overline{\mathrm{MS}}$ conventions:

$$\rho(\lambda) = \frac{1}{Z_{\text{tw} \to \overline{\mathrm{MS}}}} \rho^{\text{latt}}(Z_{\text{tw} \to \overline{\mathrm{MS}}}\lambda). \quad (38)$$

As is discussed in Ref. [9] the renormalization factor $Z_{\text{tw} \to \overline{\mathrm{MS}}}$ is given by a product of the factor $Z_{\text{tw} \to m_f}$ given

in Table IV of that reference and the factor $Z_{m_f \to \overline{\text{MS}}}$ listed in Table IV of the present paper.

Since in a lattice calculation the Banks-Casher limit of infinite volume and vanishing quark mass cannot be easily evaluated, we would like to use Eq. (37) for the case of finite volume and nonzero quark mass. However, in that case the integral over λ diverges quadratically. As a result, this equation is dominated by the region of large λ where the DWF lattice and continuum formalisms should not agree and is well outside the limited range of the 100 lowest eigenvalues which we have computed. However, much can be learned from Eq. (37) if we use it to evaluate the difference $\Delta_{l,s}$, subtracting the light and strange quark equations. This difference will be studied in Sec. IV C, comparing the subtracted spectral integral with both the simple difference of condensates, $\Delta_{l,s}$ and the improved quantity $\tilde{\Delta}_{l,s}$.

In a similar manner, the difference between the connected pseudoscalar and scalar light-quark susceptibilities, $\chi_\pi - \chi_\delta$, which serves as a good indicator of $U(1)_A$ symmetry breaking, can be expressed as a spectral integral [29]:

$$\Delta_{\pi,\delta} \equiv \chi_\pi - \chi_\delta = \int_0^\infty \mathrm{d}\lambda \rho(\tilde{m}_l, \lambda) \frac{4\tilde{m}_l^2}{(\tilde{m}_l^2 + \lambda^2)^2}, \quad (39)$$

where again this is a continuum equation which requires that all of the quantities which appear are renormalized in a consistent scheme. In contrast to Eq. (37), this expression is only logarithmically divergent and for our values of the lattice spacing and quark masses, is dominated by the region where λ is small—the region in which we have measured the spectrum and in which the lattice and continuum spectral functions should agree, except for the usual $O(a^2)$ errors inherent in a calculation at nonzero lattice spacing.

In order to distinguish and to better understand the effects of different possible behaviors of $\rho(\tilde{m}_l, \lambda)$ we will also make use of the small λ and small $\tilde{m}$ parametrization for $\rho(\tilde{m}_l, \lambda)$,

$$\rho(\tilde{m}, \lambda) = c_0 \tilde{m}^2 \delta(\lambda) + c_1 |\lambda| + c_2 \tilde{m} + \cdots, \quad (40)$$

appropriate for $T \geq T_c$ and introduced in Ref. [9]. Each term provides an ansatz for a possible behavior of $\rho(\tilde{m}_l, \lambda)$ and results in a different contribution to the susceptibility difference. In particular, $\Delta_{\pi,\delta}$ will receive three corresponding contributions:

$$\Delta_{\pi,\delta} \approx 2c_0 + 2c_1 + \pi c_2 \equiv \Delta_{\pi,\delta}^0 + \Delta_{\pi,\delta}^1 + \Delta_{\pi,\delta}^2. \quad (41)$$

Once the eigenvalue density has been computed and fit to the form assumed in Eq. (40), the resulting coefficients can be used to calculate $\Delta_{\pi,\delta}$ and discover which of these three behaviors gives the dominant contribution to the spectral integral.

In addition to allowing a quantitative measure of the relative importance of these three possible behaviors, the use of the analytic expression in Eq. (40) also allows us to potentially correct finite lattice spacing errors which may be important for small λ in our DWF formulation with finite L_s. Although much more accurate, the Hermitian DWF spectrum, like the Wilson spectrum, does not have the continuum form $\Lambda = \pm\sqrt{\lambda^2 + \tilde{m}^2}$ where $\tilde{m} = m_l + m_{\text{res}}$, at least for finite volume, finite L_s and nonzero lattice spacing. For eigenvalues Λ of D_H on the order of m_{res}, i.e. $\Lambda \lesssim 10$ MeV, we expect deviations from the continuum $\pm\sqrt{\lambda^2 + \tilde{m}^2}$ form because of residual chiral symmetry breaking. These effects do not occur if we use $\rho(\lambda)$ given by Eq. (40). In fact, comparing results obtained by direct summation over the measured spectrum with those obtained using Eq. (40) provides an estimate of the importance of these finite lattice spacing errors.

Each of the three terms in Eq. (40) corresponds to potentially interesting behavior. The λ-independent $c_2\tilde{m}$ term is expected to dominate the behavior below T_c and should describe the Banks-Casher contribution to the chiral condensate Σ_l. For $T < T_c$ the factor of $\tilde{m}$ should not appear but has been introduced here because above T_c the condensate should vanish in the limit $\tilde{m} \to 0$. As can be seen in Eq. (41), this $c_2\tilde{m}$ term will result in $\Delta_{l,s} \neq 0$ and anomalous symmetry breaking. Likewise, the linear c_1 term provides a possible mechanism for $U(1)_A$ symmetry breaking above T_c. Both the c_1 and c_2 terms are sufficiently regular as λ and $\tilde{m}$ approach 0 that they do not result in an explicit $SU(2)_L \times SU(2)_R$ symmetry breaking chiral condensate but have sufficient infrared singularity that the presence of either does result in a nonzero value for $\chi_\pi - \chi_\delta$. Thus, either term in $\rho(\lambda)$ could describe the behavior we see for $T > T_c$ where Σ_l should vanish as $\tilde{m}_l \to 0$ but $\chi_\pi - \chi_\delta$ is nonzero. As we will see, neither term appears to be present with a sufficient magnitude to describe $\chi_\pi - \chi_\delta$ for $T > T_c$.

As is discussed below, the c_0 term has the greatest relevance. This term represents the Dirac spectrum that results from the DIGA [18]. Asymptotic freedom implies that at sufficiently high temperature, the QCD partition function will be governed by weak-coupling phenomena. These should include a "dilute gas" of instantons and anti-instantons of radius $\approx 1/T$ and density $\propto \tilde{m}_l^2 \exp\{-8\pi^2/g^2(T)\}$ decreasing with increasing temperature, where $g(T)$ is the running QCD coupling constant evaluated at the energy scale T. The number of such instantons and anti-instantons is proportional to the volume and each will induce a near-zero mode in the Dirac eigenvalue spectrum. (These eigenvalues will not be exactly zero because of the overlap of the "zero"-mode wave functions associated with neighboring instantons.) The factor of $\tilde{m}^2$ in the instanton density arises from the fermion determinant for two light flavors of quarks. The
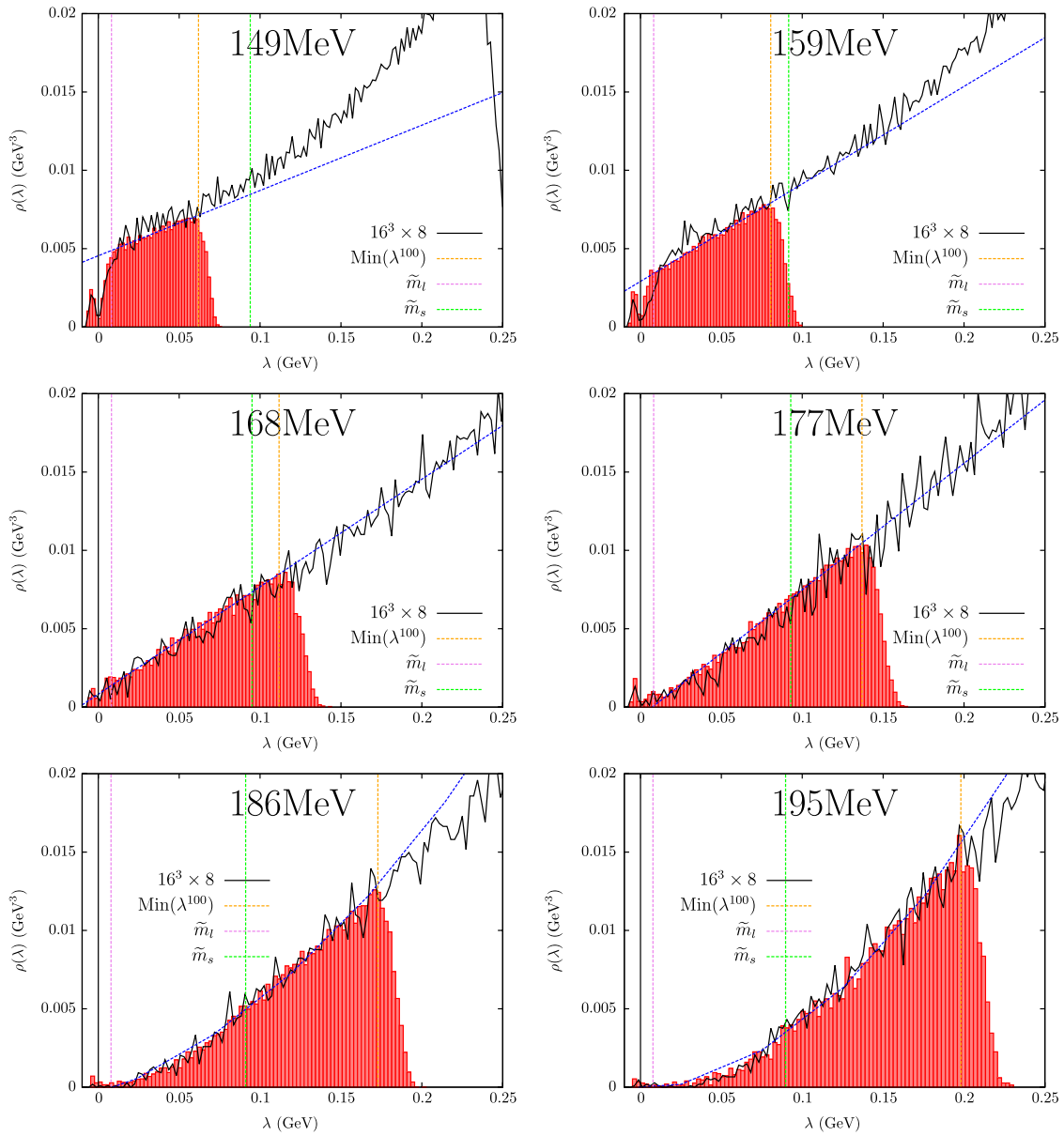
FIG. 7 (color online).   The eigenvalue spectrum for $T = 149 - 195$ MeV, expressed in the $\overline{\text{MS}}$ scheme at the scale $\mu = 2$ GeV. The imaginary, "unphysical" eigenvalues are plotted as $-\sqrt{|\Lambda^2 - \tilde{m}_l^2|}$. The spectra from the $32^3 \times 8$ ensembles are plotted as histograms and fit with a linear ($T = 149 - 178$ MeV) or a quadratic ($T = 186 - 195$ MeV) function (blue dashed line). The spectrum from each of the $16^3 \times 8$ ensembles [9] is plotted as a black solid line.

contribution of such a dilute gas of instantons and anti-instantons to the Dirac spectrum will be accurately described by the c_0 term in Eq. (40), at least for sufficiently high temperatures. As can be seen from Eq. (41), such a term will result in a nonzero value for the difference $\chi_\pi - \chi_\delta$ even in the chiral limit, $\tilde{m}_l \to 0$. The expected presence of such effects leads to the phrase "effective restoration of $U(1)_A$ symmetry," since these effects, which should appear as T becomes very large, will lead to a possibly very small but nonvanishing result of $\chi_\pi - \chi_\delta$.

As we will demonstrate in Sec. IV D we find a significant cluster of near-zero modes in the Dirac spectrum whose

number is proportional to the volume with the character-istics expected from the DIGA. We conclude that the nonzero value of $\chi_\pi - \chi_\delta$ in the region just above T_c is explained by the DIGA and that this is the dominant mechanism for our observed, nonzero breaking of $U(1)_A$ just above T_c.

B. Eigenvalue distributions

To compute the Dirac eigenvalue spectrum, we follow closely the method described in detail in Ref. [9]. The lowest 100 eigenvalues $\{\Lambda_n\}_{1 \leq n \leq 100}$ of the Hermitian DWF

Dirac operator D_H are calculated for each of ≈ 100 configurations for each of six ensembles ranging in temperature between 149 and 195 MeV using the Kalkreuter-Simma method [30]. The same fermion mass is used in the Dirac operator as was used when the ensemble was generated.

In the continuum, the eigenvalues Λ_n of the Hermitian Dirac operator have the form $\pm\sqrt{\lambda_n^2 + \tilde{m}_l^2}$ and the eigenvalue density is conventionally expressed in terms of the mass-independent eigenvalue λ. Here we will attempt to follow the same practice. However, for the DWF Dirac operator, the quark mass is not a simple additive constant but is embedded within D_{DWF} in a complex fashion. The continuum form $\pm\sqrt{\lambda_n^2 + \tilde{m}_l^2}$ is therefore not guaranteed by the structure of D_{DWF} but is expected to emerge in the limit of infinite volume, infinite L_s or vanishing lattice spacing a. Thus, in our circumstances, we will find some eigenvalues Λ_n which are smaller than $\tilde{m}_l$ and for which $\lambda_n = \sqrt{\Lambda_n^2 - \tilde{m}_l^2}$ will be imaginary. As in Ref. [9], when we present a histogram showing $\rho(\lambda)$ we include these imaginary values in a separate histogram plotted at negative λ with an imaginary value of λ added to a bin at $-|\lambda|$. Plotted in this way, these "unphysical" values of Λ are made visible and their relative importance can be judged. We exploit the symmetry between positive and negative values of λ and associate each Λ_n with magnitude greater than $\tilde{m}_l$ with the positive value $\lambda_n = +\sqrt{\Lambda_n^2 - \tilde{m}_l^2}$.

Figure 7 shows the distributions, renormalized in the $\overline{\text{MS}}$ scheme at the scale $\mu = 2$ GeV, determined from the lowest 100 eigenvalues (λ) for six ensembles at temperatures from 149 to 195 MeV. The eigenvalue densities for the $32^3 \times 8$ space-time volumes are plotted as solid histograms, while the $16^3 \times 8$ results are plotted as black, solid lines. The aforementioned imaginary, unphysical modes are plotted as $-\sqrt{|\Lambda^2 - \tilde{m}_l^2|}$ on the negative axis. The values for the total mass of light and strange quarks, $\tilde{m}_l^{\overline{\text{MS}}}$ and $\tilde{m}_s^{\overline{\text{MS}}}$, are indicated by vertical dashed lines, which give a physical scale for the eigenvalue distribution. Since we have determined only a fixed number of eigenvalues, the spectral distributions will be distorted at their upper ends. The third vertical dashed line in these plots, which appears with various x coordinates, locates the smallest value for λ_{100} found for each ensemble. The spectrum shown to the left of this line will then be undistorted by our failure to include larger eigenvalues in the figure.

Since the number of eigenmodes is proportional to the space-time volume, a fixed number of the lowest modes will become more concentrated at the lower end of the spectrum as the volume increases. This phenomena can be easily seen in Fig. 7 where the range of eigenvalues studied decreases dramatically as the space-time volume is

increased from $16^3 \times 8$ to $32^3 \times 8$. However, while the range of eigenvalues covered by the larger $32^3 \times 8$ volume is reduced, this larger volume provides a better sampling and more convincing view of the spectrum near zero, the region of greatest interest.

For $T = 149$ and 159 MeV, the eigenvalue distributions can be characterized as a linear function with a non-vanishing intercept for eigenvalues of order 10 MeV or larger. Below 10 MeV the spectrum is distorted by a combination of finite volume and residual chiral symmetry breaking effects. The nonvanishing intercept, interpreted through the Banks-Casher relation, is consistent with the nonvanishing chiral condensate and vacuum chiral symmetry breaking observed at these temperatures which lie below the pseudocritical temperature.

For $T = 168$ MeV, the linear behavior continues to be visible, but the intercept has essentially vanished, suggesting that 168 MeV is close to the pseudocritical temperature, consistent with the temperature dependence of the $SU(2)_L \times SU(2)_R$-breaking susceptibility difference $\chi_\pi - \chi_\sigma$ shown in Fig. 4.

For $T = 177$ MeV, a small peak in $\rho(\lambda)$ near the origin emerges as a cluster of near-zero modes. Such a cluster of near-zero modes might result from the Atiyah-Singer theorem and nonvanishing topological charge or from the DIGA. As is discussed below, the volume dependence of this peak and the distribution of the chirality of these modes is consistent with the DIGA and inconsistent with their arising from nonzero global topology. This small eigenvalue region can be best seen in the expanded view given in Fig. 8.

For $T = 186$ and 195 MeV, this small peak survives although it diminishes in size with increasing temperature. In addition, the peak becomes increasingly separated from the rest of the spectrum by a gap containing few eigenvalues. As a result the remainder of the spectrum, excluding this peak, can no longer be fit using a linear function. A quadratic fit is possible at $T = 186$ but an even higher power may be needed to describe the 195 MeV spectrum.

C. Subtracted chiral condensate

It is not difficult to see very approximate agreement between the intercept of the spectral density at $\lambda = 0$ (ignoring obvious distortions to the spectrum near $\lambda = 0$) and the measured value of Σ_l implied by the Banks-Casher relation. However, a careful, quantitative test of Eq. (36) must overcome two obstacles: both the finite-volume suppression of $\rho(\lambda)$ as $\lambda \to 0$ and the quadratic divergence present in Σ_q for nonzero quark mass. For a DWF calculation such a test is further complicated by the contributions of residual chiral symmetry breaking to Σ_q and $\rho(\lambda)$ for small λ. As suggested above, all of these difficulties can be overcome. The first step is to consider the subtracted chiral condensate, $\Delta_{l,s}$ defined in Eq. (4). If
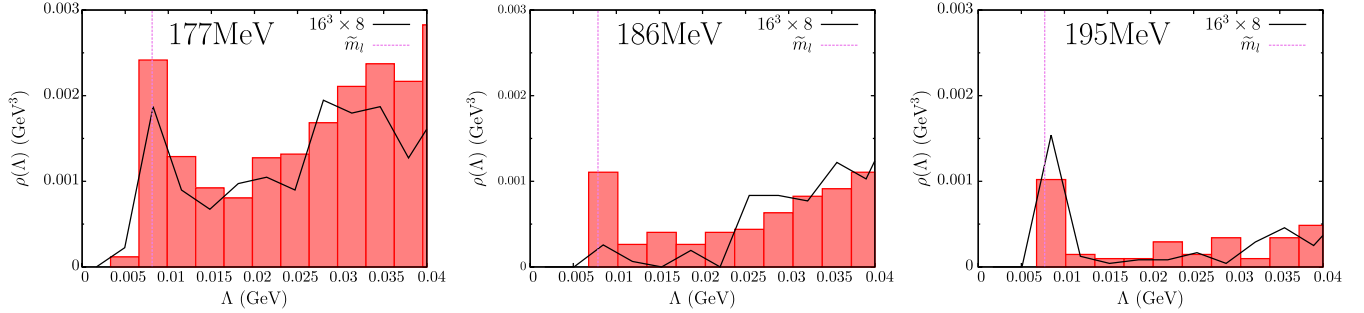
FIG. 8 (color online). (Left to right) The renormalized eigenvalue spectrum for $T = 177 - 195$ MeV without the removal of the bare quark mass. The statistics are likely insufficient for 186 MeV on the $16^3 \times 8$ ensemble; only 5 instances of "near-zero modes" are collected.

Eq. (36) is used to express $\Delta_{l,s}$ in terms of the spectral density, we obtain the more convergent result:

$$\Delta_{l,s} = \int_0^\infty d\lambda \rho(\lambda) \frac{2\tilde{m}_l(\tilde{m}_s^2 - \tilde{m}_l^2)}{(\lambda^2 + \tilde{m}_l^2)(\lambda^2 + \tilde{m}_s^2)}. \quad (42)$$

While this expression still receives a contribution from large eigenvalues, well above the group of low modes studied here, this high-mode contribution is expected to be of order $m_l m_s^2 \ln(m_s a)$ which is possibly 1% of the $(250 \text{ MeV})^3$ value of the zero temperature chiral condensate. Thus, we expect that for our present quark masses and lattice spacing, we can evaluate the right-hand side of Eq. (42) using our 100 low modes to at least a few percent accuracy, at least for $T \leq T_c$.

We can evaluate the integral in Eq. (42) using our measured eigenvalues in two ways. First for each measured configuration we can replace the integral over λ on the right-hand side of Eq. (42) by a sum over the measured eigenvalues. In addition we can express the integrand in Eq. (42) in terms of the directly measured eigenvalues Λ_n so that the uncertainties associated with those values of Λ_n lying below $\tilde{m}_l$ are avoided. The resulting expression for $\Delta_{l,s}$ becomes

$$\Delta_{l,s}^{\text{ms}} = \frac{1}{N_\sigma^3 N_\tau} \left\langle \sum_{n=1}^{100} \frac{\tilde{m}_l(\tilde{m}_s^2 - \tilde{m}_l^2)}{\Lambda_n^2(\Lambda_n^2 + \tilde{m}_s^2 - \tilde{m}_l^2)} \right\rangle, \quad (43)$$

where $\langle \ldots \rangle$ indicates an average over configurations and we use the notation "ms" (mode sum) to identify the result obtained from this summation over modes.

In the second approach to Eq. (42) we replace the spectral density $\rho(\lambda)$ by the fitted expression given in Eq. (40) and then perform the integration over λ analytically with the result:

$$\Delta_{l,s}^{\text{eig}} \equiv c_0 \tilde{m}_l + c_1 \tilde{m}_l \ln\left(\frac{\tilde{m}_s^2}{\tilde{m}_l^2}\right) + c_2 \pi \tilde{m}_l, \quad (44)$$

where terms of order $\tilde{m}_l/\tilde{m}_s$ have been neglected and the label "eig" has been introduced to distinguish this expression from those resulting from the three other approaches to the calculation of this quantity.

In Table VI we compare these two spectral methods for computing $\Delta_{l,s}$ with the results from both the direct subtraction of the measured condensates (which we continue to label as $\Delta_{l,s}$) and the improved quantity $\tilde{\Delta}_{l,s}$ which is less contaminated by residual DWF chiral symmetry

TABLE VI. Comparison of the unrenormalized results for $\Delta_{l,s}$ computed using four different methods at various temperatures and values of L_s. The data in the $16^3 \times 8, L_s = 64$ row results from a valence calculation performed on the $L_s = 48, \beta = 1.671$ (run #16) ensemble. (While these quantities are all expressed in the scheme defined by the bare lattice mass, m_q, this is not the scheme in which the eigenvalues of the five-dimensional DWF Dirac operator are defined and renormalization using the factor $Z_{\text{tw} \to m_f}$ defined in Ref. [9] has been carried out.)

#	T (MeV)	N_σ	L_s	$\tilde{m}_l$	$\tilde{m}_s$	$\Delta_{l,s}^{\text{eig}}/T^3$	$\Delta_{l,s}^{\text{ms}}/T^3$	$\Delta_{l,s}/T^3$	$\tilde{\Delta}_{l,s}/T^3$
15	149	16	32	0.00464	0.05293	6.72	6.00	3.07(12)	5.7(2)
16	149	16	48	0.00468	0.05295	6.85	5.65	5.00(10)	6.3(1)
16	149	16	64	0.00459	0.05289	$\cdots$	$\cdots$	5.57(10)	6.2(1)
2	149	32	32	0.00464	0.05293	6.45	6.39	3.84(5)	6.4(1)
3	159	32	32	0.00421	0.04856	3.86	4.28	2.83(6)	4.2(1)
5	168	32	32	0.00395	0.04490	1.64	2.19	1.46(7)	2.3(1)
6	177	32	32	0.00367	0.04165	$\cdots$	1.21	0.71(5)	1.3(1)
7	186	32	32	0.00341	0.03873	$\cdots$	0.42	0.22(4)	0.46(5)
8	195	32	32	0.00314	0.03619	$\cdots$	0.25	0.14(3)	0.30(6)

breaking effects. As can be seen from the table, for the temperatures at which the fit form given in Eq. (40) provides a good description of the eigenvalue distribution, 139 MeV $\leq T \leq$ 168 MeV, analytic integration of this three-parameter function and the direct sum over the lowest 100 modes agree reasonably well. This supports the use of the three-parameter function to provide an interpretation of our results. This agreement also suggests that the region $|\Lambda| \lesssim 10$ MeV, which is distorted in our computed Dirac eigenvalue spectrum by finite-volume and residual chiral symmetry breaking effects but treated in a fashion consistent with infinite volume, continuum expectations by the fitting function, does not play a large role in these results. The difference between $\Delta_{l,s}^{\text{eig}}$ and $\Delta_{l,s}^{\text{ms}}$ can serve as an estimate for the systematic error in the fit coefficients, a difference which at its largest is about 15%.

A second observation that can be drawn from the data in Table VI is that the quantity $\tilde{\Delta}_{l,s}$ agrees reasonably well with the result obtained directly from the Dirac spectrum over the full temperature range. This suggests that a good representation for the chiral condensate can be obtained by performing the subtraction of light and strange quark Green's functions and that in the case of DWF it is best to use the GMOR relation and subtract connected pseudoscalar susceptibilities rather than the condensates themselves which contain relatively large, uncontrolled residual chiral symmetry breaking effects. We would like to emphasize that our use of the continuum spectral Eq. (40) combined with the renormalized DWF spectrum makes strong assumptions about the validity of continuum methods in our lattice calculation at reasonably strong coupling. It is impressive that on the larger 32^3 volume, where the statistical errors are likely most reliable, Table VI shows agreement between $\Delta_{l,s}^{\text{ms}}$ and $\tilde{\Delta}_{l,s}$ consistently at the 1 sigma level, which in some cases represent an accuracy of 4% or less.

Finally we examine the results at $T = 149$ MeV where multiple ensembles with different values of L_s are available, shown in the first four lines of Table VI. Here results are shown for three values of L_s: 32, 48 and 64. As expected, the simple difference $\Delta_{l,s}$ shows a very strong dependence on L_s. While there should be substantial cancellation between the large, continuumlike modes in this difference, at the very highest energies this cancellation

will be distorted by residual chiral symmetry breaking effects. The use of the factor $(m_l + m_{\text{res}})/(m_s + m_{\text{res}})$ in the subtracted strange condensate will not, in general, cause these effects to cancel. However, this argument suggests that as L_s increases and these residual chiral symmetry breaking effects are suppressed, $\Delta_{l,s}$ should approach $\tilde{\Delta}_{l,s}$, behavior that can be seen in Table VI. Less consistent is the apparent increase in the value of $\tilde{\Delta}_{l,s}/T^3$ with increasing L_s seen on the 16^3 volume, where an increase by more than two standard deviation from 5.7(2) to 6.2(1) is seen as L_s grows from 32 to 64. Since $\tilde{\Delta}_{l,s}$ is supposed to already be close to its $L_s = \infty$ value such L_s dependence is not expected and we attribute this discrepancy to the under estimation of statistical errors for this small, 16^3 volume.

D. Near-zero modes and $U(1)_A$ symmetry

We now turn to one of the central questions addressed in this paper, the origin of the observed $U(1)_A$ symmetry breaking above T_c. We will focus on the quantity $\Delta_{\pi,\delta} = \chi_\pi - \chi_\delta$ since this difference of susceptibilities can be expressed in terms of the spectral density using Eq. (39). Table VII shows this difference at six temperatures as determined from the integrated connected Green's functions. This difference contains only a very small logarithmic singularity after multiplicative renormalization by $1/Z^2_{m_f \to \overline{\text{MS}}}$ in the continuum, $\sim (m_l + m_{\text{res}})^2 \ln m_l a$, where the sum $m_l + m_{\text{res}}$ represents schematically the effects of both the input quark mass and DWF residual chiral symmetry breaking. This controlled high-energy behavior is realized by the convergence of the integral in Eq. (39), even when $\rho(\lambda)$ increases linearly or quadratically with λ.

Therefore, in Table VII we also show the contributions to the spectral integral in Eq. (39) of each of the three separate ansätze in Eq. (40), given in Eq. (41). Some cells are left blank because the corresponding behavior cannot be seen in the spectral data. For example, at $T \leq 168$ MeV, there is no visible accumulation of near-zero modes that might be described by a $\delta(\lambda)$ term in $\rho(\lambda)$. However, at $T \geq$ 177 MeV and above we can count a number of near-zero modes that form a small but visible peak in $\rho(\lambda)$ near $\lambda = 0$. Assuming a Poisson distribution, we take the square root of the total number of these near-zero modes as a rough estimate of errors for the corresponding contribution. Similarly the

TABLE VII. A comparison of $\Delta_{\pi,\delta}$ measured from the difference of correlation functions with the three contributions computed from fitting the eigenvalue density to the expression in Eq. (40) and with the result $\Delta_{\pi,\delta}^{\text{ms}}$ obtained from the mode sum given in Eq. (45), for the $32^3 \times 8$ ensembles. All results are renormalized in the $\overline{\text{MS}}(\mu = 2$ GeV) scheme.

#	T (MeV)	β	$\tilde{m}_l$	N_{cfg}	$\Delta_{\pi,\delta}^0/T^2$	$\Delta_{\pi,\delta}^1/T^2$	$\Delta_{\pi,\delta}^2/T^2$	$\Delta_{\pi,\delta}^{\text{ms}}/T^2$	$\Delta_{\pi,\delta}/T^2$
2	149	1.671	0.00464	158	$\cdots$	3.7(3)	76(2)	109	87(2)
3	159	1.707	0.00421	109	$\cdots$	4.6(1)	42(1)	70	60(2)
5	168	1.740	0.00395	83	$\cdots$	4.9(1)	11(1)	35	35(2)
6	177	1.771	0.00367	170	23(1)	5.0(1)	$\cdots$	25	23(2)
7	186	1.801	0.00341	171	8(1)	$\cdots$	$\cdots$	8	6(1)
8	195	1.829	0.00314	76	7(1)	$\cdots$	$\cdots$	6	6(2)

constant contribution or intercept has vanished for $T \geq$ 177 MeV and above $T = 177$ MeV the linear term is also difficult to determine and the eigenvalue density is dominated by what appears to be quadratic behavior.

We can also determine the susceptibility difference $\Delta_{\pi,\delta}$ by using a direct sum over modes as was done for $\Delta_{l,s}$ in Eq. (43) and tabulated as $\Delta_{l,s}^{\text{ms}}$ in Table VI. Examining the continuum spectral equation (39), we can write an expression for $\Delta_{\pi,\delta}$ analogous to that in Eq. (43) for $\Delta_{l,s}$:

$$\Delta_{\pi,\delta}^{\text{ms}} = \frac{1}{N_\sigma^3 N_\tau} \left\langle \sum_{n=1}^{100} \frac{2\tilde{m}_l^2}{\Lambda_n^4} \right\rangle. \tag{45}$$

The results from this mode sum are shown in the second column from the right in Table VII where very good agreement is seen with the explicit difference of correlation functions. This substitution of our renormalized DWF eigenvalue spectrum directly into the continuum equation for $\Delta_{\pi,\delta}$ is a stringent test of that spectrum. The infrared singular factor $1/\Lambda_n^4$ appearing in Eq. (45) might have shown large, unphysical fluctuations associated with configuration-by-configuration fluctuations in residual chiral symmetry breaking. In fact, it is possible that the larger values shown in Table VII for $\Delta_{\pi,\delta}^{\text{ms}}$ relative to the actual correlator difference $\Delta_{\pi,\delta}$ at the two lowest temperatures are a result of this effect. However, overall the agreement between $\Delta_{\pi,\delta}^{\text{ms}}$ and $\Delta_{\pi,\delta}$ is remarkably good.

The separate contributions to $\Delta_{\pi,\delta}$ presented in Table VII give a clear, quantitative description of how the contribution of each piece evolves as the temperature increases. For $T \leq T_c$, the constant, or Banks-Casher term, gives the major contribution to $\Delta_{\pi,\delta}$. In contrast, in the region above the pseudocritical temperature, the delta-function term dominates and its contribution alone agrees well with the result from the difference of integrated correlators. We conclude that the nonzero $U(1)_A$ symmetry breaking that we observe above T_c in the correlator difference $\chi_\pi - \chi_\delta$ results from this small cluster of near-zero modes which can be seen in the spectral distributions shown in Fig. 7 for $T = 177$, 186 and 195 MeV and more easily in the expanded plots in Fig. 8.

It is possible that these near-zero modes become exact zero modes in the continuum limit and are a result of

nonzero global topology and the Atiyah-Singer theorem. If this is the case, the number of these zero modes should increase in proportion to $\sqrt{V}$ with increasing space-time volume. Thus, for zero modes resulting from nonzero global topology we expect the corresponding density per space-time volume to be proportional to $1/\sqrt{V}$. Were such exact zero modes the only contribution to $U(1)_A$ symmetry breaking then we would conclude that $U(1)_A$ symmetry will be restored in the limit of infinite volume.

However if we compare the results for 32^3 (solid red histograms) and 16^3 (black lines) in the expanded view of these peaks shown in Fig. 8[2] for $T = 177$, 186 and 195 MeV, we easily see that the density is volume independent, instead of shrinking by a factor of $\sqrt{8}$ as the volume is increased from 16^3 to 32^3. Thus, the volume dependence of these near-zero modes corresponds to what is expected if they result from a relatively dilute gas of instantons and anti-instantons whose number, and whose corresponding near-zero modes, will grow proportional to the volume.[2]

We have also examined the chirality of these near-zero modes. In particular, if these modes are the result of nonzero global topology, then, for a single configuration, all these modes should be of the same chirality, that of the global topological charge ν. If ν is positive then each of the zero modes should be right handed and in our DWF case have support primarily on the right-hand, $s = L_s - 1$ boundary. If ν is negative then all modes should be left handed and their wave functions should be largest on the left-hand, $s = 0$ boundary. In contrast, if these modes arise from a dilute instanton gas, they are produced by a mixture of instantons and anti-instantons and the chirality of each mode should have an equal probability to be either positive or negative within a single configuration.

We choose the $T = 177$ MeV ensemble to study the chirality of the near-zero modes since it has the most near-zero modes among the three highest temperature ensembles, where these modes are seen. We did not save the full five-dimensional eigenfunctions when computing the lowest 100 modes and have available only values for the squared modulus of the five-dimensional wave function, integrated over the left- and right-hand wall for each mode. Therefore we define the chirality of the nth mode as

$$\chi_n = \frac{\int d^4x \bar{\Psi}_n(x,0)(1+\gamma^5)\Psi_n(x,0) - \int d^4x \bar{\Psi}_n(x,L_s-1)(1-\gamma^5)\Psi(x,L_s-1)}{\int d^4x \bar{\Psi}_n(x,0)(1+\gamma^5)\Psi(x,0) + \int d^4x \bar{\Psi}_n(x,L_s-1)(1-\gamma^5)\Psi(x,L_s-1)}, \tag{46}$$

which compensates for the fact that even for a chirality eigenstate, the five-dimensional wave function will not be localized solely on one of the four-dimensional walls but will spread into the fifth dimension. If we examine the zero modes, we find that some of them have chirality near zero. This might be expected for a not-too-dilute instanton gas

where the two modes of a nearby instanton-anti-instanton pair will mix so that neither have a definite chirality,

---

[2]Here we use the distributions of Λ instead of λ near the origin, since it allows us to ignore the large relative fluctuations in these small eigenvalues below $\tilde{m}_l$.
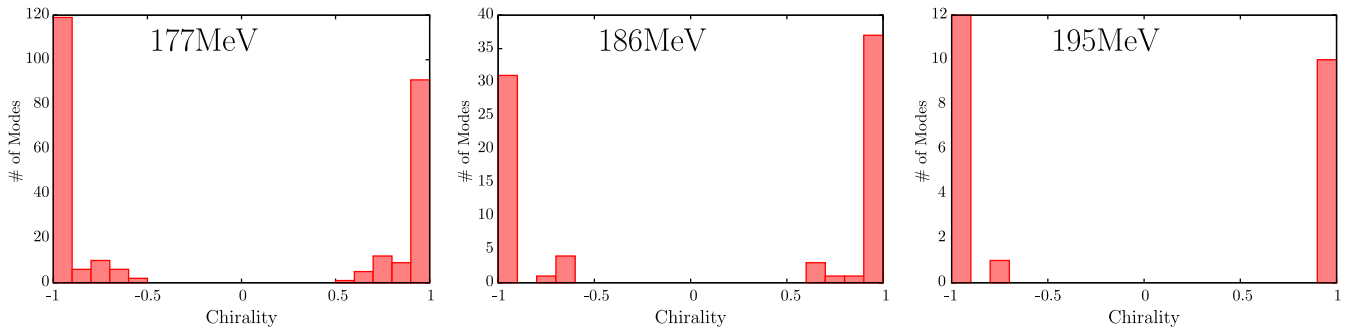
FIG. 9 (color online). (Left to right) The distribution of chiralities for the near-zero modes at the three temperatures $T = 177$, 186 and 195 MeV and the $32^3 \times 8$ volume. Here we only use modes lying in the first four histogram bins in Fig. 8 which corresponds to $\Lambda \lesssim 12.5$ MeV.

However, such behavior could also be the result of our strong coupling and gauge configurations with changing topology producing zero modes of uncertain chirality. As a result we choose to examine only those near-zero modes whose chirality is greater than 0.7 in magnitude. The effects of this choice choice can be seen in Fig. 9 where we plot the histogram of the near-zero modes for $T = 177$, 186 and 195 MeV. It appears that at these temperatures, almost all of the near-zero modes are localized on one of the two four-dimensional walls and thus have a chirality very close to $+1$ or -1. Our restriction that the magnitude of the chirality is greater than 0.7 captures approximately 95% of the near-zero modes. Figure 9 suggests that this concentration of chirality at ± 1 increases with increasing temperature. Determining whether this apparent trend is the result of (i) limited statistics at the higher temperatures, (ii) increasing spatial localization of the zero modes and therefore less mixing as T increases or (iii) better defined gauge field topology at weaker coupling requires further study.

Table VIII lists the number of configurations which have N_0 near-zero modes, N_+ of which have positive chirality. Those modes included in the counts presented in Table VIII must lie in the peak region (first four bins) shown in Fig. 8, with Λ at or below approximately 12.5 MeV and with a

chirality of magnitude 0.7 or greater. A binomial distribution consistent with the DIGA describes the data in a more convincing way than the bimodal distribution that would be seen for the exact zero modes resulting from nonzero global topology.

We conclude that the agreement between the value of $\Delta_{\pi,\delta}$ measured from the difference of correlators and the delta-function contribution $\Delta^0_{\pi,\delta}$ shown in Table VII implies that the anomalous breaking of chiral symmetry for $T > T_c$ results from these near-zero modes. Further, the volume dependence and chirality distribution of the modes making up this delta-function contribution gives strong evidence that the nonzero anomalous symmetry breaking found above T_c is the result of a dilute gas of instantons and anti-instantons and that no new mechanism of anomalous symmetry breaking is needed.

V. CONCLUSIONS

We have extended earlier finite-temperature QCD studies [9] from $16^3 \times 8$ to larger $24^3 \times 8$ and $32^3 \times 8$ volumes, all performed using a 200 MeV pion mass and the chiral, DWF lattice action. Significant dependence on volume is seen for both the chiral condensate, Σ_l, and the disconnected chiral susceptibility, χ_{disc}, for temperatures below T_c. Most dramatic is the large decrease in χ_{disc} below T_c as the volume is increased from 16^3 to 24^3 and 32^3 which is shown in the left panel of Fig. 5. Without data at one or more additional values of the light-quark mass, we are unable to make a proper comparison of this finite-volume dependence with the predictions of $O(4)$ universality. However, on a qualitative level this behavior is predicted by finite-volume $O(4)$ scaling [14] and was anticipated by the results given in Ref. [16]. Here a model calculation is presented using renormalization group methods applied to a theory including fundamental quarks, gluons and mesons. Since the volume dependence of this theory should be consistent with $O(4)$ universal behavior, the results in Ref. [16] can be viewed as a prediction of $O(4)$ universal finite-volume behavior which is now evident in our lattice calculation. We expect to make a quantitative comparison

TABLE VIII. The number of configurations found in the 177 MeV (run #6) ensemble with given values for the total number (N_0) of near-zero modes and total number (N_+) of those modes with positive chirality. We consider only modes with $\Lambda \leq$ 12.5 MeV and a chirality whose magnitude exceeds 0.7. The distribution is clearly different from the bimodal distribution $N_+ = N_0$ or 0 expected if these near-zero modes were induced by nonzero global topology and the Atiyah-Singer theorem.

$N_+ \backslash N_0$	0	1	2	3	4	5
$N_0 = 1$	40	29	$\cdots$	$\cdots$	$\cdots$	$\cdots$
$N_0 = 2$	11	20	12	$\cdots$	$\cdots$	$\cdots$
$N_0 = 3$	3	11	6	2	$\cdots$	$\cdots$
$N_0 = 4$	0	1	2	1	0	$\cdots$
$N_0 = 5$	0	2	0	0	0	0

with finite-volume $O(4)$ scaling when the HotQCD $32^3 \times 8$ and $64^3 \times 8$, $m_\pi = 135$ MeV data can be included in the analysis.

A second result presented here is the observation of nonvanishing $U(1)_A$ symmetry breaking above T_c and its quantitative connection to the density of near-zero Dirac eigenvalues. The volume dependence of these near-zero modes and the failure of their chiralities to be correlated per configuration matches precisely the expectation of the dilute instanton gas approximation. This might also be called the dilute caloron gas approximation if we recognize the finite-temperature distortions that are expected for instantons at finite temperature whose space-time extent approaches the length $1/T$ [31–35]. (For a thorough review of the subject of instantons in QCD, including their effects at finite temperature, see Ref. [36].) While more study of the space-time structure of these zero modes is required to completely establish this picture of $U(1)_A$ symmetry breaking, our results are all well explained by this mechanism.

The possible $U(1)_A$ symmetry breaking above T_c was recently analyzed theoretically by Aoki, *et al.* using a lattice regularization, based on overlap fermions [37]. We also refer the reader to this paper for a discussion of and references to earlier theoretical work on the question of $U(1)_A$ symmetry breaking above T_c and its relation to the Dirac eigenvalue spectrum. Among the conclusions of Ref. [37] is that $\chi_\pi - \chi_\delta$ vanishes in the limit of infinite volume and vanishing quark mass for $T > T_c$. We have found a nonzero value for $\chi_\pi - \chi_\delta$ on the smallest, 16^3 volume which becomes larger when the volume was increased eightfold to 32^3. While we have examined only a single quark mass, we believe that this mass is sufficiently small as to be a good approximation to zero. We believe this to be the case because the explicit $SU(2)_L \times SU(2)_R$ symmetry breaking effect of the quark mass on the difference $(\chi_\pi - \chi_\delta) - (\chi_\sigma - \chi_\eta)$ is significantly smaller than the scale of $\chi_\pi - \chi_\delta$. (We are now studying a second, smaller mass to test this assertion.) However, our results and the arguments presented in Ref. [37] can be made consistent if those arguments are reversed to conclude that the analyticity in $\tilde{m}_l^2$ assumed above T_c in Ref. [37] is not present.

There is also a potential conflict between our results and the conclusions of a recent 2-flavor study of Cossu, *et al.* [13] on a $16^3 \times 8$ volume using overlap fermions. Reference [13] reaches the conclusion that there is a gap in the Dirac eigenvalue spectrum and degeneracy between the π and δ correlators above T_c. However, the numerical evidence supporting their conclusion is strongest at relatively high temperatures where our results also show few small Dirac eigenvalues and small (but significant) results for $\chi_\pi - \chi_\delta$. Given our larger volumes and our smaller light-quark mass, which is fixed in physical units, it is possible that the small effects which we are able to extract may not be visible in this first overlap study.

Especially interesting is the failure of this overlap calculation to see the small peaks in the Dirac spectrum near $\lambda = 0$ found in our DWF work. As is pointed out by Cossu, *et al.*, residual chiral symmetry breaking in a DWF calculation does distort the small eigenvalue region. However, while this distortion may shift individual eigenvalues by a few MeV, it is not expected to create near-zero modes that are not present in the continuum theory. Our detailed comparisons of the predictions of spectral formulas with the improved chiral condensate suggest that the averaged features of the Dirac spectrum, even for $\lambda \sim 1$ MeV, are accurate. We believe that this absence of a near-zero mode peak in the overlap data has at least two possible explanations. First since the size of these peaks is very temperature dependent, even a 10% underestimate of the energy scale for the overlap relative to the DWF simulation could explain their absence in the former. Second, the elimination of topology change in the overlap simulation results in a nonergodic evolution algorithm which may distort the thermal distribution of near-zero modes, especially at weaker couplings and smaller dynamical quark masses, in spite of the evidence to the contrary.

The study of 16^3, 24^3 and 32^3 volumes in this work gives us a good understanding of the effects of finite volume and a very interesting opportunity to compare with the predictions of $O(4)$ universality. By working at relatively small light-quark mass on a line of constant physics ($m_\pi = 200$ MeV), we believe that the effects of explicit chiral symmetry breaking present are small and that the evidence for anomalous symmetry breaking just above $T_c \approx 160$ MeV is strong. This symmetry breaking decreases rapidly as the temperature grows making the signal difficult to see at our highest temperature, 196 MeV. The study of the Dirac eigenvalue spectrum suggests that this $U(1)_A$ symmetry breaking results from near-zero modes whose characteristics match well with those predicted by the dilute instanton gas approximation. However, it is important to verify this picture by extending the investigation to even smaller light-quark mass and larger volumes. Calculations currently being carried out by the HotQCD Collaboration on $32^3 \times 8$ and $64^3 \times 8$ volumes with $m_\pi = 135$ MeV should resolve these remaining uncertainties.

ACKNOWLEDGMENTS

[1] R. D. Pisarski and F. Wilczek, Phys. Rev. D **29**, 338 (1984).

[2] A. Butti, A. Pelissetto, and E. Vicari, J. High Energy Phys. 08 (2003) 029.

[3] A. Pelissetto and E. Vicari, Phys. Rev. D **88**, 105018 (2013).

[4] E. Meggiolaro and A. Morda, Phys. Rev. D **88**, 096010 (2013).

[5] P. M. Vranas, arXiv:hep-lat/0001006.

[6] P. M. Vranas, Phys. Rev. D **74**, 034512 (2006).

[7] H. Fukaya, S. Hashimoto, K.-I. Ishikawa, T. Kaneko, H. Matsufuru, T. Onogi, and N. Yamada (JLQCD Collaboration), Phys. Rev. D **74**, 094505 (2006).

[8] D. Renfrew, T. Blum, N. Christ, R. Mawhinney, and P. Vranas, *Proc. Sci.*, LATTICE2008 (**2008**) 048.

[9] A. Bazavov *et al.* (HotQCD Collaboration), Phys. Rev. D **86**, 094503 (2012).

[10] P. Chen *et al.*, Phys. Rev. D **64**, 014503 (2001).

[11] M. Cheng, N. H. Christ, M. Li, R. D. Mawhinney, D. Renfrew, P. Hegde, F. Karsch, M. Lin, and P. Vranas, Phys. Rev. D **81**, 054510 (2010).

[12] S. Borsanyi, Y. Delgado, S. Dürr, Z. Fodor, S. D. Katz, S. Krieg, T. Lippert, D. Nógrádi, and K. K. Szabó, Phys. Lett. B **713**, 342 (2012).

[13] G. Cossu, S. Aoki, H. Fukaya, S. Hashimoto, T. Kaneko, H. Matsufuru, and J.-I. Noaki, Phys. Rev. D **87**, 114514 (2013).

[14] J. Engels and F. Karsch, arXiv:1402.5302.

[15] J. Engels, S. Holtmann, T. Mendes, and T. Schulze, Phys. Lett. B **514**, 299 (2001).

[16] J. Braun, B. Klein, and P. Piasecki, Eur. Phys. J. C **71**, 1576 (2011).

[17] C. G. Callan, R. Dashen, and D. J. Gross, Phys. Lett. **63B**, 334 (1976).

[18] D. J. Gross, R. D. Pisarski, and L. G. Yaffe, Rev. Mod. Phys. **53**, 43 (1981).

[19] M. Cheng, N. Christ, S. Datta, J. van der Heide, C. Jung *et al.*, Phys. Rev. D **77**, 014511 (2008).

[20] L. S. Brown, R. D. Carlitz, and C. Lee, Phys. Rev. D **16**, 417 (1977).

[21] M. Gell-Mann, R. J. Oakes, and B. Renner, Phys. Rev. **175**, 2195 (1968).

[22] V. Furman and Y. Shamir, Nucl. Phys. **B439**, 54 (1995).

[23] T. Blum, P. Chen, N. H. Christ, C. Cristian, C. Dawson *et al.*, Phys. Rev. D **69**, 074502 (2004).

[24] N. H. Christ and L. L. Wu, Nucl. Phys. B, Proc. Suppl. **106–107**, 438 (2002).

[25] Y. Aoki *et al.* (RBC Collaboration and UKQCD Collaboration), Phys. Rev. D **83**, 074508 (2011).

[26] A. Bazavov, T. Bhattacharya, M. Cheng, C. DeTar, H. Ding *et al.*, Phys. Rev. D **85**, 054503 (2012).

[27] T. Banks and A. Casher, Nucl. Phys. **B169**, 103 (1980).

[28] L. Giusti and M. Luscher, J. High Energy Phys. 03 (2009) 013.

[29] S. Chandrasekharan and N. H. Christ, Nucl. Phys. B, Proc. Suppl. **47**, 527 (1996).

[30] T. Kalkreuter and H. Simma, Comput. Phys. Commun. **93**, 33 (1996).

[31] B. J. Harrington and H. K. Shepard, Phys. Rev. D **17**, 2122 (1978).

[32] B. J. Harrington and H. K. Shepard, Phys. Rev. D **18**, 2990 (1978).

[33] T. C. Kraan and P. van Baal, Phys. Lett. B **428**, 268 (1998).

[34] T. C. Kraan and P. van Baal, Nucl. Phys. **B533**, 627 (1998).

[35] K.-M. Lee and C.-h. Lu, Phys. Rev. D **58**, 025011 (1998).

[36] T. Schaefer and E. V. Shuryak, Rev. Mod. Phys. **70**, 323 (1998).

[37] S. Aoki, H. Fukaya, and Y. Taniguchi, Phys. Rev. D **86**, 114512 (2012).